Redox upconversion and electrocatalytic cycles in activation of Si-Si bonds: diverging reactivity in hole- and electron-catalyzed transformations

Victoriya A. Balycheva,[1] Beauty K. Chabuka,[2] Leah R. Kuhn,[2] Pavel G. Shangin,[1] Anna Ya. Akyeva,[1] Irina V. Krylova,[1] Victor A. Korolev,[1]Andrey V. Lalov, [1] Mikhail P. Egorov,[1] Igor V. Alabugin,[2] Mikhail A. Syroeshkin[1]**

[1] N.D. Zelinsky Institute of organic chemistry, 119991, Moscow, Russia, syroeshkin@ioc.ac.ru

[2] Department of Chemistry and Biochemistry, Florida State University, Tallahassee, Florida 32306, United States, alabugin@chem.fsu.edu

Abstract. Electron transfer is a powerful tool for promoting chemical reactions. A subset of redox-mediated transformations are “electroneutral” reactions, where the reactant and product are in the same oxidation state. In such processes, electrons (or holes) can serve as genuine catalysts if the products have higher reduction (or oxidation) potential than the reactants, i.e. in the presence of electron (or hole) upconversion.

This work explores the differences between electron and hole catalysis in redox-activated transformations of the same substrate. We show that for redox upconversion to occur in both the reductive and oxidative mode, the reduced and oxidized reactions must follow different paths. The chosen substrate, 1,2-disila-3,5-cyclohexadiene **1**, combines an electron-rich π-system with a Si-Si bond can undergo Si-Si bond scission in both the oxidative and reductive regimes. Single electron oxidation with a molecular oxidant leads to the formation of a radical cation that undergoes an intramolecular rearrangement with the elimination of dimethylsilylene and the formation of a radical cation of silole, **2**. The latter can oxidize another molecule of neutral reactant **1**, a step that closes the hole catalytic cycle. The unique utility of radical-cationic reactivity mode is illustrated by the lack of hole-upconversion under electrochemical conditions where the radical cationic reaction path is aborted by further oxidation at the electrode.

In contrast, the radical anion formed from one-electron reduction of **1** is unreactive. This persistent species can be formed reversibly in THF, both chemically and electrochemically. Its reactivity can be unlocked by the addition of stoichiometric amounts of water. Although the subsequent reaction also involves Si-Si bond cleavage, it follows a path that is different from the radical-cationic version. Interestingly, electrochemical experiments clearly confirm that this process is also a chain reaction that requires catalytic amount of electrons (0.3 equiv.) for the complete conversion of the substrate. Computations identify a possible mechanistic pathway to the observed products and support the importance of reductant upconversion for this electron-catalyzed process.

Hence, this work identified the first molecular system that can undergo true electron-catalyzed and hole-catalyzed processes and confirmed that these processes lead to different products.

Keywords. Organosilicon electrochemistry, cyclic voltammetry, silicon-silicon bond cleavage, electron catalysis, hole catalysis, electron upconversion, hole upconversion.

Graphical abstract

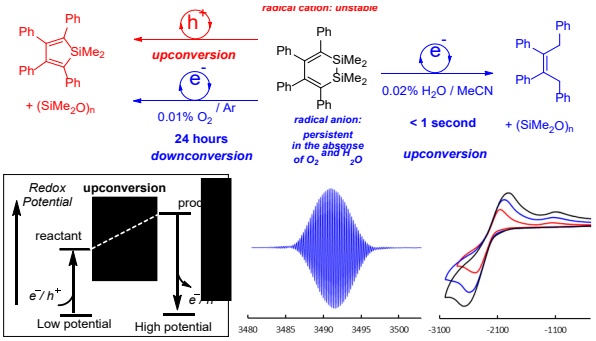

1. Introduction

Electron transfer serves as a powerful tool for promoting chemical reactions.[1,2,3,4,5,6,7] As expected, many of these reactions lead to either oxidation or reduction. However, a subset of redox-mediated transformations are “electroneutral” reactions, where the reactant and the product are in the same oxidation state. In such reactions, addition of an electron or hole is temporary and the “borrowed” electron/hole is transferred to an external agent at the end of reaction. If the electron/hole can be transferred from the product radical ion to a fresh molecule of the neutral starting material, the overall transformation becomes a self-propagating chain reaction where electrons and holes serve as true catalysts.[8,9,10] A thermodynamic requirement for this process is that a product radical ion should be a more powerful reducing/oxidizing agent than the reactant radical ion. In other words, electron and hole catalysis require electron and hole upconversion.

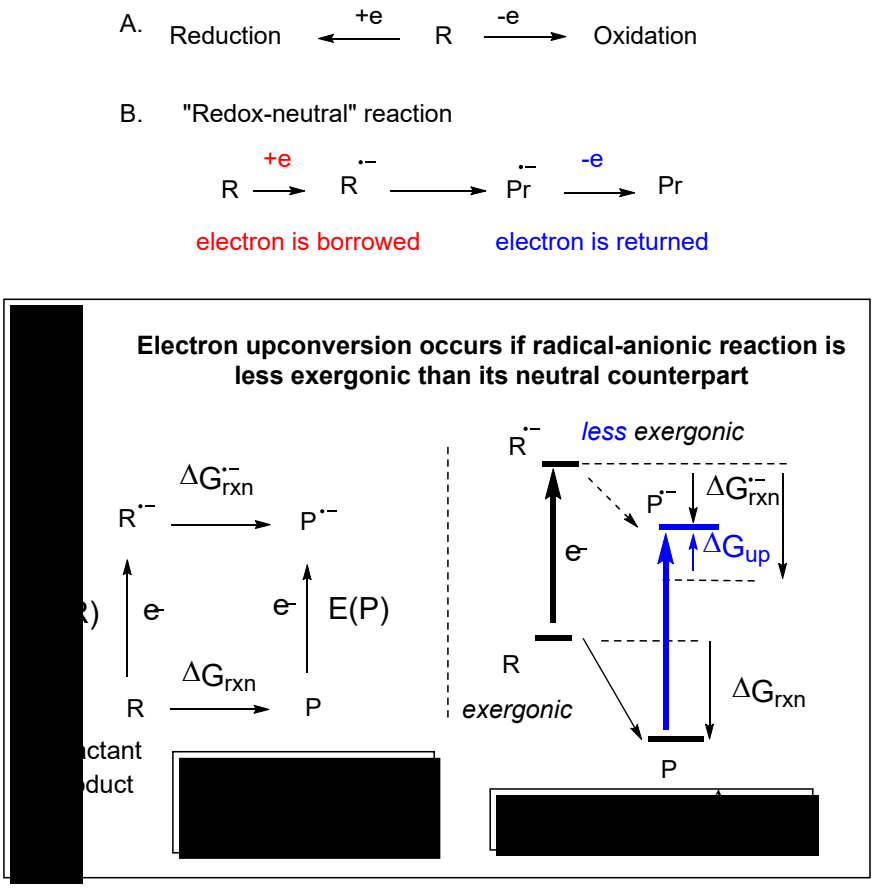

Scheme 1. Two types of reactions mediated by electron transfer: A) Oxidation and reduction lead to change in the oxidation state of the substrates. B) “Redox-neutral” reactions retain the oxidation state because addition of an electron or hole happens temporarily. C) Thermodynamic cycle for converting reaction exergonicity to reductant upconversion.

This may seem an impossible requirement because a simple electron transfer process is exergonic only when it converts a stronger oxidant (or reductant) into a weaker oxidant or reductant. If electron transfer is the only process, the decrease of redox potential for a process that decreases free energy of the system is unavoidable, because change in reduction potential simply reflects change in energy per unit charge. However, the situation changes when chemical bonds are formed and broken simultaneously with charge transfer. In such cases, reactions can be thermodynamically favorable while producing strongly reducing/oxidizing species from weakly reducing/oxidizing reactants. Previously, we have explained this seeming paradox by showing how part of reaction exergonicity can be converted into increase in the redox potential. In a closed thermodynamic cycle, the difference in exergonicity of neutral and radical ionic reaction *has to* translate directly in change in the redox potential for the product radical ion relative to the reactant radical ion (Scheme 1C). We have coined the term “reductant upconversion” or “electron upconversion” for such processes under reductive conditions [11] and “oxidant upconversion” or “hole upconversion” under oxidative conditions (Scheme 2).[12]

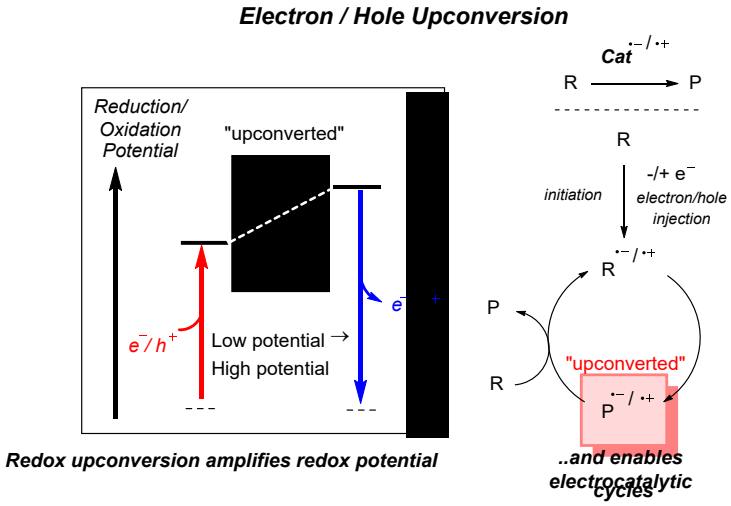

Scheme 2. (Left) The paradox of redox upconversion, where a reactant with a lower redox potential is converted into a product with a higher redox potential. (Right) Redox upconversion creates efficient hole/electron catalyzed electrocatalytic cycle where the radical ion of the product can transfer the catalytic hole (or a catalytic electron) to the fresh molecule of reactant, restarting the catalytic cycle.

The concept of redox upconversion as a thermodynamic prerequisite of efficient redox catalytic cycles is relatively new. The scope and limitations of reductive upconversion were systematically analyzed only recently, whereas the intriguing possibility of analogous oxidative upconversion remains very scarcely documented.[13] Electron upconversion is not rare. In fact, it is *expected* for associative reactions between a radical and an anion. It can serve as a reliable tool in designing reactions as illustrated by a variety of bond-forming reactions that proceed under mild conditions (Scheme 3A).[14,15,16,17,18]

In this work, we focus on more challenging dissociative redox upconversion. Fragmentations are common in redox reactions as electron transfer often weakens chemical bonds. In particular, removal of an electron from a bonding orbital during oxidation can weaken a chemical bond contributing to the HOMO. In a similar way, the injection of an extra electron during reduction can weaken a chemical bond when the LUMO has contributions from the relevant antibonding orbital. A common result of such redox activation is fragmentation of the initially formed radical ion along the weakened bond, followed by a cascade of subsequent transformations of ionic and radical intermediates.

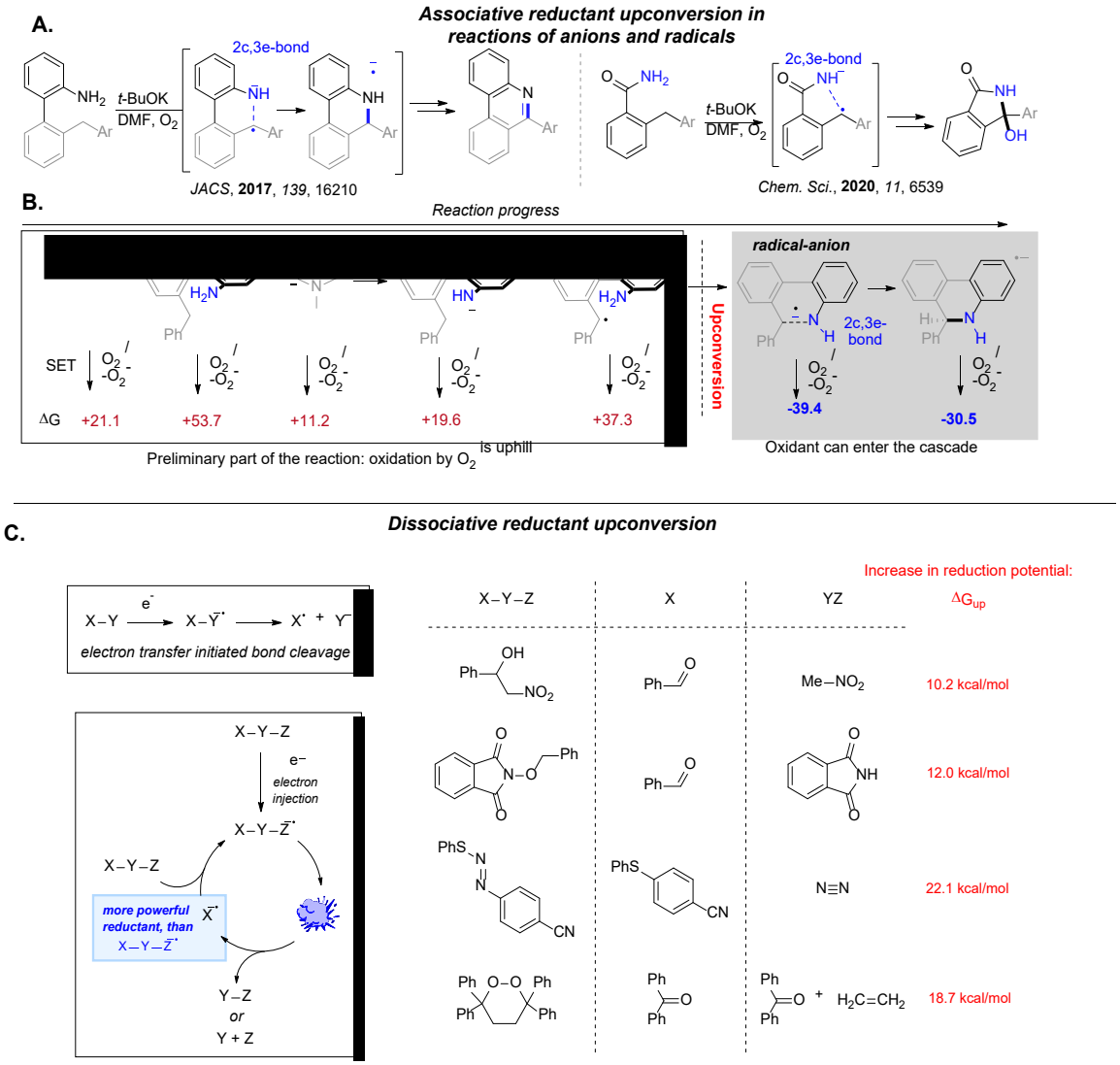

Scheme 3. A) Two examples of associative reductant upconversion for C-H amination mediated by molecular oxygen. B) The utility of reductant upconversion in controlling the timing for the oxidation step in a multistep reaction in the presence of anions, radicals, and an oxidant. C) The principle of dissociative reductant upconversion and examples of electron transfer initiated bond cleavage.

A corollary of this well-known behavior is that *reductive* X-Y fragmentations generally involve systems with the relatively low-lying σ^*_{X-Y} antibonding orbitals whereas the oxidative X-Y fragmentations involve systems with the relatively high energy σ_{X-Y} bonding orbitals. Reductive fragmentations via electron upconversion typically involve bonds with electronegative elements such as oxygen and nitrogen in N-O bond in the N-benzyloxyphthalimide[19], O-O bonds in cyclic peroxides,[20] or S-N bond in azosulfide radical anions[21] (Scheme 3C). Electron upconversion in fragmentation of C-C bonds next to acceptor groups in 1-phenyl-2-nitroethanol radical anion[22] are also known. Such fragmentations produce the upconverted product radical anions that are much more reducing agents (0.44-0.88 V) than the reactant radical anions.

On other hand, oxidative fragmentations are expected to be observed for bonds with *electropositive* elements. These general expectations suggest that a comparison of redox catalyzed transformations of the ***same*** substrate in the oxidative and reductive regimes

may be difficult. However, such comparison would be interesting from a fundamental point of view because even if both redox catalytic cycles initiate bond cleavage as the initial stage, the subsequent stages *cannot be expected to be identical*, if both cascades must proceed through an electrocatalytic chain mechanism with redox upconversion. In general, if one takes a pair of compounds (i.e., the reactant and the product of a chemical reaction), the one that is easier to reduce is also the one that is *harder* to oxidize (**Scheme 4**). Hence, if the product radical *anion* is *more* reducing than the reactant radical anion, the product radical *cation* is likely to be *less* oxidizing than the reactant radical cation.

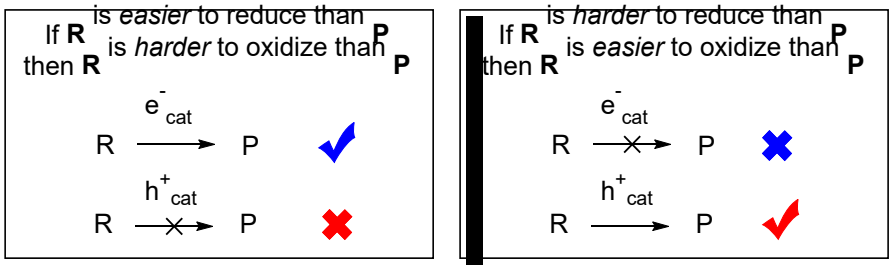

Scheme 4. Synthetic complementarity of the two redox approaches: cascades mediated by hole- and electron catalysis are unlikely to give the same product.

So, if bonds containing electronegative elements are easy to reduce while bonds with electropositive elements are easy to oxidize, what kind of "chameleonic" substrate would be easy to reduce *and* oxidize? The answer is "weak bonds", especially longer bonds with heavy elements. Such bonds generally have low σ/σ* separation, so they can be both a good donor and a good acceptor.[23] Indeed, Scheme 5 illustrates that the σ^*_{Si-Si} orbital is also relatively low (between σ^*_{O-N} and σ^*_{N-N} and much lower than σ^*_{N-N} and σ^*_{C-C} orbitals in the model substrates) while at the same time, the σ_{Si-Si} is relatively high in energy (higher than the all of the other σ-orbitals shown in Scheme 5). These notable features suggest that the same Si-Si bond may be broken in both the oxidative and the reductive regimes.

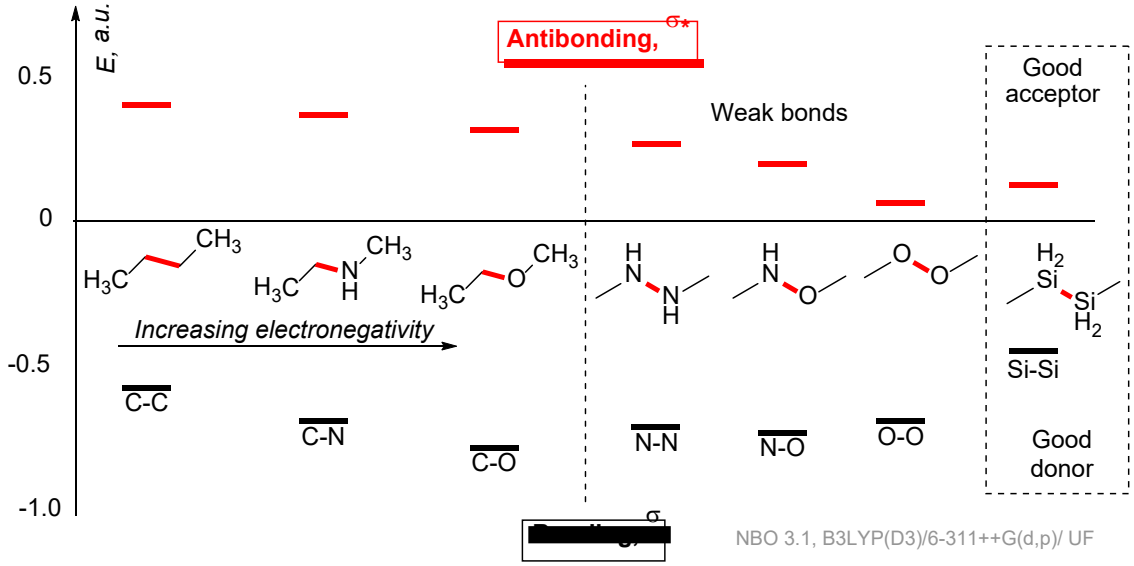

Scheme 5. The calculated natural bonding orbital (NBO) energy of bonding (σ-orbitals) and antibonding (σ*-orbitals) for bonds potentially involved in electron transfer initiated bond cleavage.

From this point of view, molecules with a Si-Si bond provide an intriguing structural motif for the fundamental studies of the upconversion processes in redox-mediated reactions. Furthermore, such compounds are of general interest in chemistry as the closest analogs of organic compounds, for which catenation and the presence of C-C bonds are typical. They are also of practical interest, due to their specific electronic and redox properties[24,25,26,27] promising for photonics,[28] microelectronics,[29] molecular wires design,[30,31,32] etc. As the Si-Si bond is more labile than the C-C bond, redox catalysis may be broadly applicable in this molecular family.

This work will compare the two modes of redox catalysis (i.e., single electron oxidation and reduction) for disilacyclohexadiene **1** (**Scheme 6**). Its oxidative ring contraction into a silole derivative **2** has been reported [33,34] but its mechanism has not been studied in detail and it was unclear if hole upconversion is important. Furthermore, the radical-anionic chemistry of **1** has not been studied before. Most importantly, there are no examples of reductant upconversion and catalysis by electrons associated with breaking the Si-Si bond. Hence, testing if any of the two upconversion modes is possible in this system became the first subject of this study.

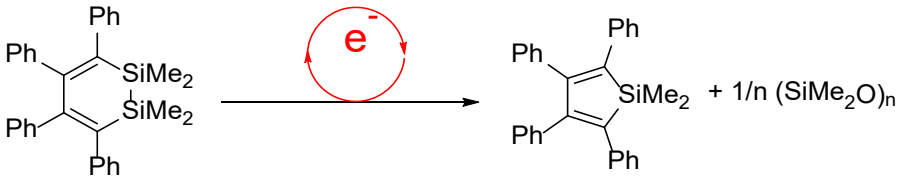

1 **2**

Scheme 6. Possible electrochemical transformation of disilacyclohexadiene **1**.

2. Methods

2.1. Materials and Synthetic procedures

The 1,1-dimethyl-2,3,4,5-tetraphenylsilole (**2**) and 1,1,2,2-tetramethyl-3,4,5,6-tetraphenyl-1,2-disila-3,5-cyclohexadiene (**1**) were synthesized as described previously.[35,36] Their structure and purity were confirmed by ^{1}H, ^{13}C and ^{29}Si NMR spectroscopy, mass-spectroscopy and elemental analysis. The samples were stored in a dry argon-filled glove box with water and oxygen contents below 0.1 ppm before using.

Synthesis of 1,2,3,4-tetraphenylbutene-2. In the glovebox, 414 mg (1 mmol) of 1,1-dimethyl-2,3,4,5-tetraphenylsilole **2** was dissolved in 20 ml of dry THF, after which 23 mg (1 mmol) of sodium was added. The solution quickly acquires a lilac color. The mixture was left to stir for 48 hours. Then a 2% solution of water in THF was added dropwise to the solution until the lilac color completely disappeared. The resulting yellow solution was evaporated, the solid residue was extracted three times with 20 ml of petroleum ether, and the extracts were combined. The mixture is passed through silica gel, then evaporated to a volume of about 5 ml and placed in the freezer. After 48 hours, the solution was separated from the precipitated crystals of the starting **2**, the crystals were washed with ice-cold petroleum ether, and the washing was added to the solution. The solution is evaporated under vacuum, the product is a viscous yellowish mass, yield 25%. The structure of the product was confirmed by ^{1}H and ^{13}C NMR and HRMS. *NMR* (THF, δ) ^{1}H: 7.2-6.7 (m, 20H, Ar), 4.01 (s, 4H, CH_2). ^{13}C: 142.97 (C), 139.61 (C), 138.23 (C), 129.95 (CH Ar), 128.50 (CH Ar), 128.13 (CH Ar), 127.32 (CH Ar), 125.79 (CH Ar), 125.72

(CH Ar), 40.5 (CH_2). HRMS (ESI): found 378.2201, calculated for [$C_{28}H_{24}+NH_4^+$]$^+$ 378.2216; found 383.1758, calculated for [$C_{28}H_{24}+Na^+$] 383.1770; found 399.1500, calculated for [$C_{28}H_{24}+K^+$] 399.1510.

Experiment with EtBr. The experiment was held in glovebox. In NMR tube a solution of 12 mg (0.25 mmol) **1** and 0.3 mg (30 mol% eq.) potassium in 0.5 ml THF was prepared. After 1 day all the solution became red, the radical anion was formed. The tube was placed without lid into a gas chamber with 1 ml EtBr on bottom. After 2 days the solution became pale yellow, the tube was retrieved, closed with lid and parafilm, spectra were obtained (Figure S2).

Experiment with I_2. The experiment was held in glovebox. In NMR tube a solution of 12 mg (0.25 mmol) **1** and 0.3 mg (30 mol% eq.) potassium in 0.5 ml THF was prepared. After 1 day all the solution became red, the radical anion was formed. The tube was placed without lid into a gas chamber with iodine crystals (~200mg, >>1eq.) on bottom. After 2 days the solution became pale yellow, the tube was retrieved, closed with lid and parafilm, spectra were obtained (Figure S3).

Experiment with PCl_3. The experiment was held in glovebox. In NMR tube a solution of 12 mg (0.25 mmol) **1** and 0.3 mg (30 mol% eq.) potassium in 0.5 ml THF was prepared. After 1 day all the solution became red, the radical anion was formed. The tube was placed without lid into a gas chamber with 1 ml PCl_3 on bottom. After 2 days the solution became bright orange and gel like, the tube was retrieved, closed with lid and parafilm, spectra were obtained (Figure S4).

Experiment with TsOH. The experiment was held in glovebox. In NMR tube a solution of 12 mg (0.25 mmol) **1** and 1 mg (100 mol% eq.) potassium in 0.5 ml THF was prepared. After 1 day all the solution became red, the radical anion was formed. The 1 ml 2% solution of TsOH (~1.1 eq.) in THF was added within a few seconds. The red color changed to yellow, and a large amount of TsOK as a precipitate was formed. 1 day later spectra were obtained (Figure S5).

Experiment with tetracyanoethylene. The experiment was held in glovebox. In NMR tube a solution of 12 mg (0.25 mmol) **1** and 0.4 mg (40 mol% eq.) potassium in 0.5 ml THF was prepared. After 1 day all the solution became red, the radical anion was formed. The 1% solution of TCNE in benzene was added dropwise using micropipette into the tube for 30 min until the content became yellow solution with violet precipitate. 1 day later spectra were obtained (Figure S6).

2.2. Photolysis experiments

NMR tube was filled in glovebox with 1.5 ml of dried over molecular sieves benzene and 100 mg **1**, then under resin tube, locked with forceps, was retrieved from box, degassed under vacuum and, keeping vacuum inside, sealed. Reference NMR spectra obtained. A DRSh-500 high-pressure Hg lamp (500 W) with water filter (to prevent IR sample heating) was used for photolysis. NMR tube with the solution has been photolyzed for 7 hours, each 15 min the tube was shaken, each 2 hours NMR spectra were obtained to control the reaction. After 7 hours less than 5% of **1** was in the sample, the photolysis was stopped, as over exposition led to tetraphenylsilol deposition in the mixture. NMR spectra showed the molar ratio for mixture components: **4** : **3** : **2** : **1** = 7 : 16 : 1.5 : 1. NMR

tube was heated in water bath for 5 hours 70 °C. After, NMR spectra were obtained, molar ratio of components was **4** : **2** : **1** : **3** = 50 : 3 : 2 : 0. The tube was opened in glovebox, the solvent was evaporated, the product was a viscous pale-yellow mass, well soluble in benzene, THF, hexane. As all the attempts to recrystallize it failed, the mass was used as was. The yield, obtained via integral comparison of ^{1}H spectra peak (as the tube was sealed no solvent evaporation was possible, peaks were compared with the satellite of benzene), was 90% (main impurities – unreacted **1** and **2**).

4. ^{1}H NMR, δ ppm (C_6H_6): 7.35-6.7 (m, 20H, Ar), 0.74 (s, 6H, CH_3, $^{2}J_{Si-H}$=6.1Hz), 0.51 (s, 6H, CH_3, $^{2}J_{Si-H}$=5.8=Hz). ^{29}Si NMR, δ ppm (C_6H_6): +40.8. ^{13}C NMR, δ ppm (C_6H_6): 140.36, 138.5, 136.9, 129.6, 129.4, 127.3, 125.4, 124.1, 47.2 (C_{bridge}, $^{1}J_{Si-C}$=39Hz), 1.31, -4.4.

3. ^{1}H NMR, δ ppm (C_6H_6): 7.35-6.7 (m, 20H, Ar), 0.48 (s, 3H, $Si_{silirane}$-CH_3, $^{2}J_{Si-H}$=6.8Hz), 0.39 (s, H, Si-CH_3, $^{2}J_{Si-H}$=6.8Hz), 0.37 (s, 3H, $Si_{silirane}$-CH_3, $^{2}J_{Si-H}$=8.1Hz), 0.21 (s, 3H, Si-CH_3, $^{2}J_{Si-H}$=7.9Hz). ^{29}Si NMR δ ppm (C_6H_6): -38 ($Si_{silirane}$), +22 ($Si_{pentacycle}$). ^{13}C NMR δ ppm (C_6H_6): 140 (=C-Si), 129.6, 129.4, 127.3, 125.3, 124.1, 55.8 ($C_{silirane}$), 32.4 (Si-C-Si), 1.3, -4.4, -4.8.

2.3. NMR / HRMS / GC/MS / X-Ray

^{1}H NMR (300 MHz) and ^{13}C NMR (75 MHz) were recorded in protic (non-deuterated) solvents on Bruker Avance-300, and ^{29}Si (60 MHz) – on Bruker AM300 at ambient temperature. NMR spectra were referenced using the signal of protio solvent (for ^{1}H NMR), the dominant solvent signal (for ^{13}C NMR), and Me_4Si signal (for ^{29}Si NMR). EPR spectra were recorded with a Bruker EMX 6/1 (9.8 GHz) spectrometer, coupled with an ER 4102ST resonator.

High resolution mass spectra (HRMS) were measured on a Bruker micrOTOF II instrument using electrospray ionization (ESI). The measurements were done in a positive ion mode (interface capillary voltage 4.5 kV); mass range from *m*/*z* 50 to *m*/*z* 1600; external or internal calibration was done with ESI Tuning Mix, Agilent. A syringe injection was used for the solutions in methanol (flow rate 3 μl min^{-1}). Nitrogen was applied as a dry gas (flow rate 4 l min^{-1}); the interface temperature was set at 180 °C.

In GC/MS TRACE GC ULTRA chromatograph with a DSQ II quadrupole mass spectrometric detector equipped with a capillary column 30 m long and 0.25 mm inner diameter was used. TR-5MS 0.25 μm thick was used as an active phase. The carrier gas was helium supplied at a rate of 1.2 ml/min. The injector temperature was 280 °C, the starting column temperature was 70 °C (2 min), the final column temperature was 280 °C (10 min), and the temperature rise rate was 15 °C/min. For mass spectrometric detection, an ionization energy of 70 eV was set.

X-ray diffraction data were collected at 100 K on a four-circle Rigaku Synergy S diffractometer equipped with a HyPix6000HE area-detector (kappa geometry, shutterless ω-scan technique), using graphite monochromatized Cu $K_α$-radiation. The intensity data were integrated and corrected for absorption and decay by the CrysAlisPro program.[37] The structure was solved by direct methods using SHELXT[38] and refined on F^2 using SHELXL-2018[39] in the OLEX2 program.[40] All non-hydrogen atoms were refined with

individual anisotropic displacement parameters. All hydrogen atoms were placed in ideal calculated positions and refined as riding atoms with relative isotropic displacement parameters. A rotating group model was applied for methyl groups.

2.4. Cyclic voltammetry and controlled potential electrolysis

Oxidation and reduction behavior of **1** and **2** was analyzed by cyclic voltammetry using a digital potentiostat IPC-Pro-MF (Econix). The solutions preparation and all measurements were made in an argon-filled glove box with water and oxygen contents below 0.1 ppm. Before that, acetonitrile (HPLC grade, Acros) and tetrahydrofuran (HPLC grade, Acros), with initial water content of <100 ppm, were stored over 4 Å molecular sieves preliminarily dried under oil-pump vacuum at 200-250 °C for 4 hrs. Bu_4NBF_4 (Sigma Aldrich) was dried under oil-pump vacuum at 80 °C for 4 hrs. The water content in Bu_4NBF_4/MeCN did not exceed 10 ppm, and in Bu_4NBF_4/THF did not exceed 5 ppm as determined by Karl Fischer titration using a Mettler-Toledo Titrator C10SD. The compounds **1** and **2** dissolved in the supporting electrolyte with a concentration of $5 \cdot 10^{-3}$ M were electrochemically tested in a standard three-electrode glass cell at a potential sweep rate of 100 mV s^{-1}. The working electrode was a glassy carbon disc electrode with a diameter of 1.7 mm. Before using, it was polished with abrasive paper and then GOI paste until the surface attained a mirror shine. The counter electrode was a Pt wire pre-annealed in a gas burner flame to remove oxides and other possible contaminations. The potentials of the studied processes were measured versus the Ag wire coated with AgCl (prepared by galvanostatic anodizing in 5% HCl solution) separated from the bulk electrolyte solution by an electrolytic bridge filled with the supporting electrolyte. The reference electrode was calibrated versus the ferrocene/ferrocenium redox couple. Also ferrocene was used as standard to establish a one-electron current level under the experimental conditions.

When performing controlled potential electrolysis, the counter electrode was separated from the cathode electrolyte solution by a diaphragm in the same way as the reference electrode. The working electrode was a glassy carbon rod (d = 1.7 mm) immersed in the solution by 3 cm. The cathode electrolyte solution was stirred during the electrolysis. The decrease in the substrate concentration in the solution was monitored by the i/t-curve, as well as using cyclic voltammetry.

2.5. Quantum chemical calculations

All quantum chemical calculations were performed by the ORCA [41,42,43] ver. 5.0.2 program package using a hybrid PBE0 [44] density functional in a triple-zeta basis set with two polarization functions def2-TZVPP [45] and atom-pairwise dispersion correction with the Becke-Johnson damping scheme (D3BJ) [46,47]. All calculations were performed in acetonitrile unless specified, using the implicit conductor-like polarizable continuum model (CPCM). TightSCF convergence criteria were applied throughout. RI-J and “chain of spheres” COSX approximation [48] with the def2/J auxiliary basis set [49] was used to speed up calculations. Full geometry optimization with TightOpt convergence criteria was carried out to find stationary points on the potential energy surfaces. Numerical harmonic frequency calculations were used to obtain thermodynamic quantities and verify that all

stationary points found were local minima. Visualization of molecular orbitals were produced using the ChemCraft 1.8 program.[50,51] Electronic structures and properties were analyzed by Natural Bond Orbitals (NBO, Version 3.1) [52] analysis implemented in Gaussian09.

3. Results & Discussion

3.1. General considerations and comparison of radical-cation and radical-anion formation

As a starting point, let us inspect the frontier Molecular Orbitals (FMOs) of **1**. Calculations reveal that the HOMO is significantly localized at the Si-Si σ-bond while the LUMO has large contributions from the diene π-system, with no bonding character on the Si-Si bond. The MOs suggest that resulting products are likely to be different for the two regimes and that the oxidation is more likely to result in Si-Si bond cleavage.

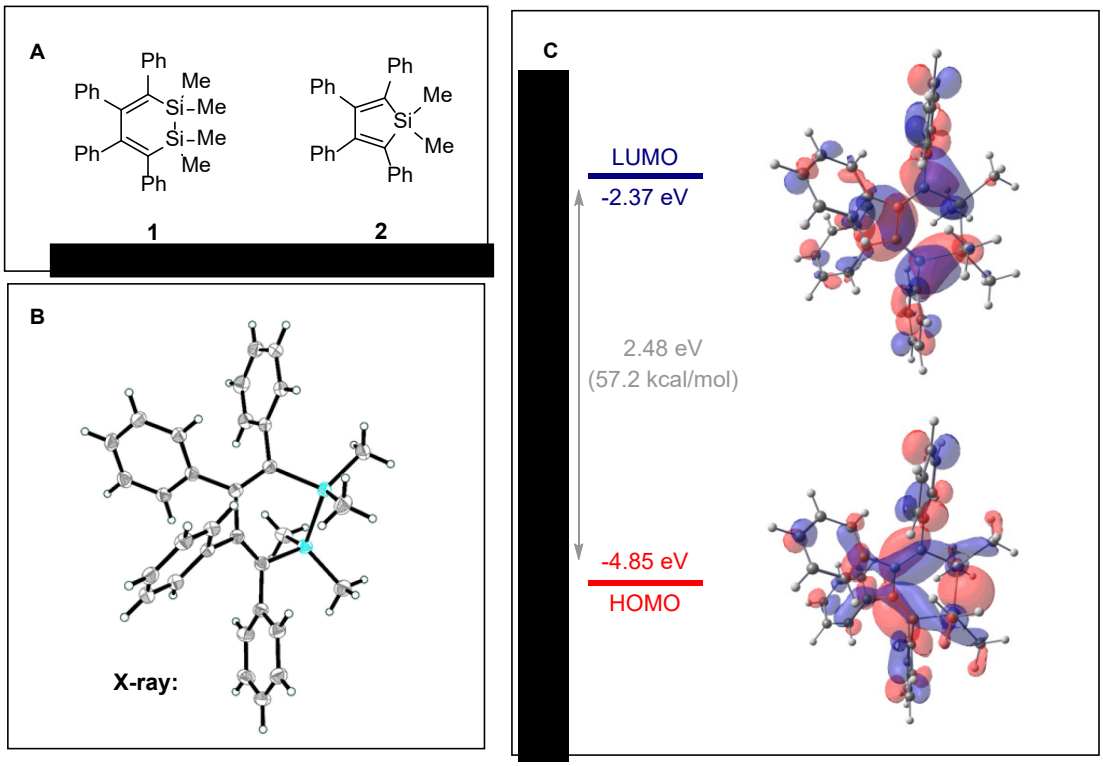

Figure 1. A. Structures of compounds **1** and **2** (panel A). X-ray structure (panel B) and frontier Molecular Orbitals (FMOs) of compound **1** (Panel C).

We also compared the redox potentials of these molecules. The voltametric curves of oxidation and reduction of **1** and **2** on a glassy carbon working electrode in 0.1 M Bu_4NBF_4/acetonitrile solution are shown in **Figure 2**. In addition, summarized in the table are the oxidation (E^p_{ox}) and reduction (E^p_{red}) peak potentials, and the differences (ΔE^p), including the energies of the longest-wavelength transitions in the UV-Vis spectra. In agreement with the principle presented in **Scheme 4**, hole upconversion would be observed during transformation of $\mathbf{1}^{+\cdot}$ into $\mathbf{2}^{+\cdot}$, while electron upconversion will not occur for the analogous transformation of the two radical-anions.

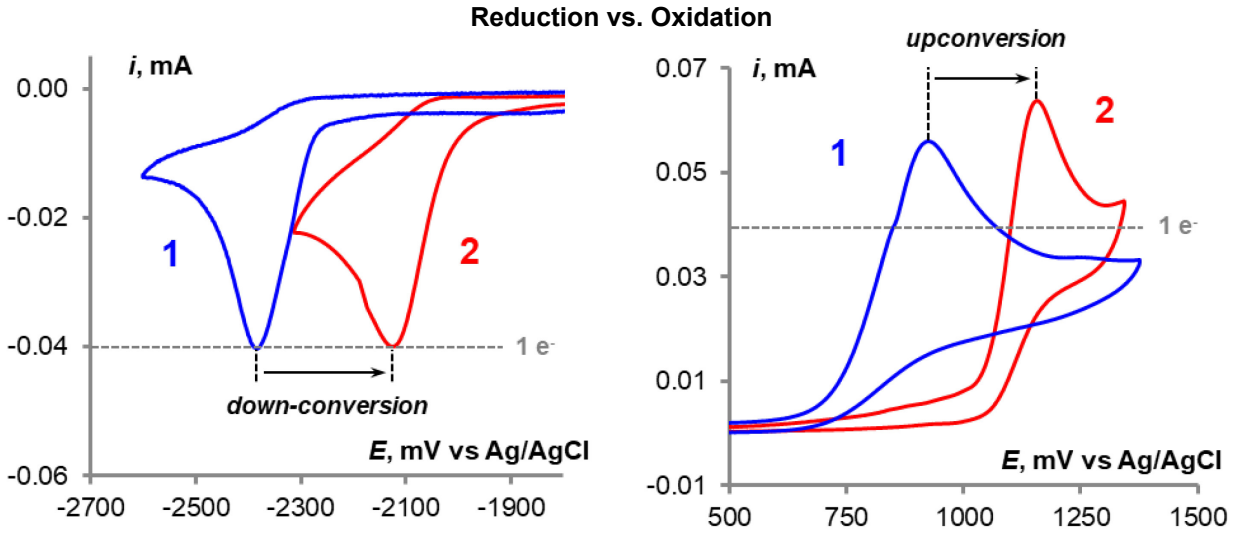

Compound	E^{p}_{ox}, V	E^{p}_{red}, V	ΔE^{p}, V	h^{ν}, nm (eV)
1	0.890	-2.379	3.269	340 (3.65)[34]
2	1.155	-2.125	3.280	361 (3.44)[34]

Figure 2. CV curves for **1** and **2** with table summarizing the reduction and oxidation peak potentials , including their differences in comparison with HOMO/LUMO transitions in UV spectra. The voltammograms were recorded in 0.1 M Bu_4NBF_4/MeCN electrolyte (water content < 10 ppm / 0.5 mM) on a glassy carbon disc electrode at a scan rate of 100 mV/s. The concentration of the analytes is 5 mM in both cases (upconversion is only possible if **1** is converted into **2** in the oxidative regime).

Intrigued by the differences between the two redox processes, we proceeded to explore their chemical outcomes. Although it was already reported that single electron oxidation initiates the ring contraction in disilahexadienes **1** with the formation of a silole derivative **2**, [53,54] the role of hole catalysis in this process was not explored. To our knowledge, the chemistry associated with one-electron reduction of **1** has not been explored.

3.2. Oxidation

The formation of **2** during single electron oxidation of **1** was discussed in the literature using chemical oxidants such as $(4\text{-}BrC_6H_4)_3NSbCl_6$ (47% yield in CH_2Cl_2, substrate/oxidant ratio not given).[33] In the photochemical version, the reaction was studied in the presence of catalytic amounts of (10%) methylene blue (59% yield in Bu_4NBF_4/MeCN) [33] and C_{60} (65% yield in benzene/benzonitrile after 10 hours of irradiation with 21% conversion) as photosensitizers.[34] Once excited, each of the sensitizers becomes a sufficiently strong electron acceptor to oxidize **1**. Because the sensitizer's radical anion is a powerful reductant, it may give the electron back to the radical cation of the product. Although this step regenerates the photocatalyst, it also prevents electron transfer from the neutral reactant to the oxidized product (a condition for establishing a true hole-catalyzed process). Hence, the involvement of redox upconversion in photoredox processes can be suppressed. In general, the catalytic cycle based on hole upconversion is absent, the reaction will need an influx of photons to keep the catalytic cycle repeating itself.

A plausible radical cation mechanism in the absence of photocatalysis is shown in **Scheme 7**. Oxidation of **1** produces the radical cation **A**. The Si-Si bond in a disilane is generally quite weak and contributes significantly to the HOMO. As a result, single electron oxidation is followed by rapid Si-Si cleavage with the formation of the distonic radical cation **B**. [55] The latter species contains a highly electrophilic center Si^+ that can readily attack the double bond.[56] This attack forms a five-membered intermediate **C**, stabilized by the β-Si effect.[57,58,59,60] Elimination of dimethylsilylene would produce the radical cation **D**, which is the product of one-electron oxidation of **2**. **D** is a more powerful oxidant than **A**, and therefore can easily oxidize unreacted **1** in the bulk solution. This hole transfer step closes the catalytic cycle by converting **D** into neutral product **2**, and, at the same time, generating a new equivalent of the reactant radical cation **A**.

A priori, one can also consider the possibility of hole-catalyzed conversion of **1** into **2** by intramolecular rearrangement of **A** to **D** with the elimination of dimethylsilylene, bypassing the stages of formation of **B** and **C** as kinetically independent particles. Regardless of which of the two scenarios are correct, each of them would be accompanied by oxidant upconversion as follows from the relative oxidation potentials of **1** and **2**. Based on these potentials, hole transfer from **D** to **1** is exergonic.

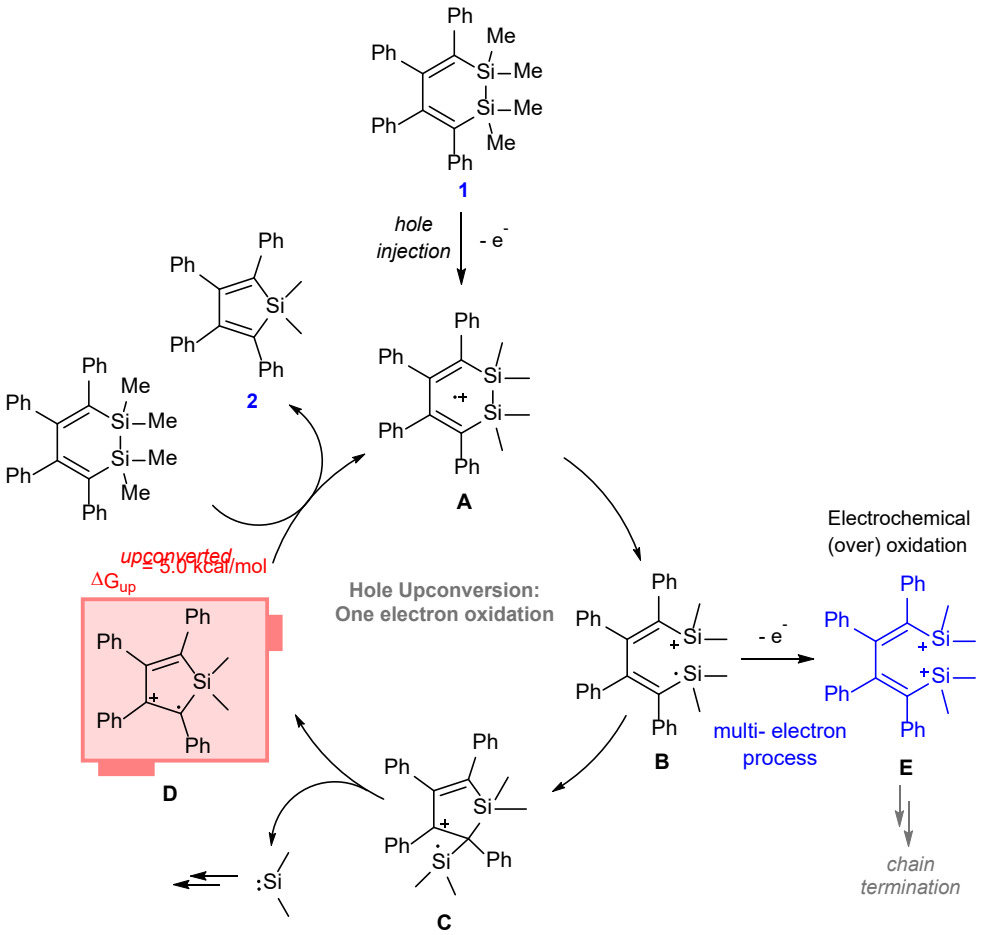

Scheme 7. Transformations of **1** into **2** via single electron oxidation. Note that oxidation of Si-radical center in **B** intercepts it and diverts to a different path.

Disrupting chain process by overoxidation:

Unfortunately, the sequence of transforming **1** to **2** cannot be reproduced via electrochemical activation. Most likely, this is a consequence of overoxidation of the key intermediate **B** with the disruption of the catalytic cycle. Based on the literature data, the oxidation potential of **B** to **E** has to be lower than the oxidation potential of **1** to **A**.[55] Hence, the electrochemically produced silicon-centered radicals (i.e., formed via ring opening of a disilane) should be readily oxidized to the respective cations more easily. Dication **E** is a super-reactive particle capable of entering into a variety of chemical reactions, including with the media, etc.

For a chemical oxidant, the instability of the initial radical cation towards further oxidation does not prevent the involvement of **B** in the catalytic cycle. This is simply due to the low probability of simultaneous encounter of molecule **1** with two molecules of the oxidant under the typical experimental conditions. In contrast, electrochemical oxidation occurs in the near-electrode space, where sequential oxidation that makes the transformation of **B** into **E** inevitable, is much more likely.

Indeed, the direct electrochemical oxidation does not lead to transformation of **1** into **2**. If the *silole derivative* **2** were formed, the electrooxidation curve of compound **1** would show not only a peak at 0.89 V (oxidation of **1**), but also a peak in the region of 1.15 V (oxidation of **2**). However, the experiments do not show the 1.15 V peak (*Figure* 1). Furthermore, the hole-catalyzed **1**-to-**2** conversion is a process requiring catalytic amounts of oxidant. Therefore, during its course, a decrease in the current of the oxidation peak of **1** relative to the level corresponding to 1 e^- per molecule should be observed. However, the corresponding current is significantly larger than 1 e^- suggesting ECE ('electrochemical-chemical-electrochemical') mechanism. [61]

Alternatively, it could be suggested that the rearrangement of **A** to **D** may be relatively slow on the voltammetry time scale. However, in this case, one would expect the chemical reversibility of the oxidation peak of **1**. Instead, the oxidation peaks of both **1** and **2** are completely irreversible, which indicates that the respective radical cations undergo rapid further chemical transformations under the experimental conditions (Bu_4NBF_4/MeCN).

Taken together, these data provide a valuable lesson in the design of hole-catalyzed processes. On one hand, the hole catalyzed conversion of **1** to **2** is a clear example of hole upconversion as a more powerful oxidant **D** is formed from a weaker oxidant **A**. The 0.26 V difference in potentials between **A** and **D** corresponds to 5.0 kcal/mol hole upconversion that should be sufficient for running an efficient hole-catalytic cycle. Indeed, the oxidative transformation of **1** into **2** proceeds well in the chemical version. However, the catalytic cycle is interrupted as the reaction follows a different path (the **A**-**B**-**E** mechanism in **Scheme 7** in the electrochemical version. Oxidation is necessary but overoxidation derails the catalytic cycle*!*

3.3. Reduction

Unlike oxidation processes, the reductive transformations of **1** via the formation of its radical anion, as far as we know, has not been reported in the literature. From Figure *2* the possible cyclopentadiene product **2** has a lower reductive potential than reactant **1**, indicating reductant upconversion is not possible if product **2** is generated by the

reduction of **1** (i.e., the transformation **1**→**2** corresponds to the model presented in **Scheme 4** on the right).

As shown in Figure 2, compound **1** is reduced in acetonitrile by a one-electron mechanism based on the corresponding peak current. This process is chemically irreversible, i.e., the radical anion **F,** formed from **1**, is unstable, likely due to the interaction with acetonitrile. Indeed, when the solvent is changed to THF, the reduction curves of **1** become chemically highly reversible even at relatively low potential scan rates (>50 mV/s). For comparison, Figure 3 shows the CV curves of **2** recorded under the same conditions.*

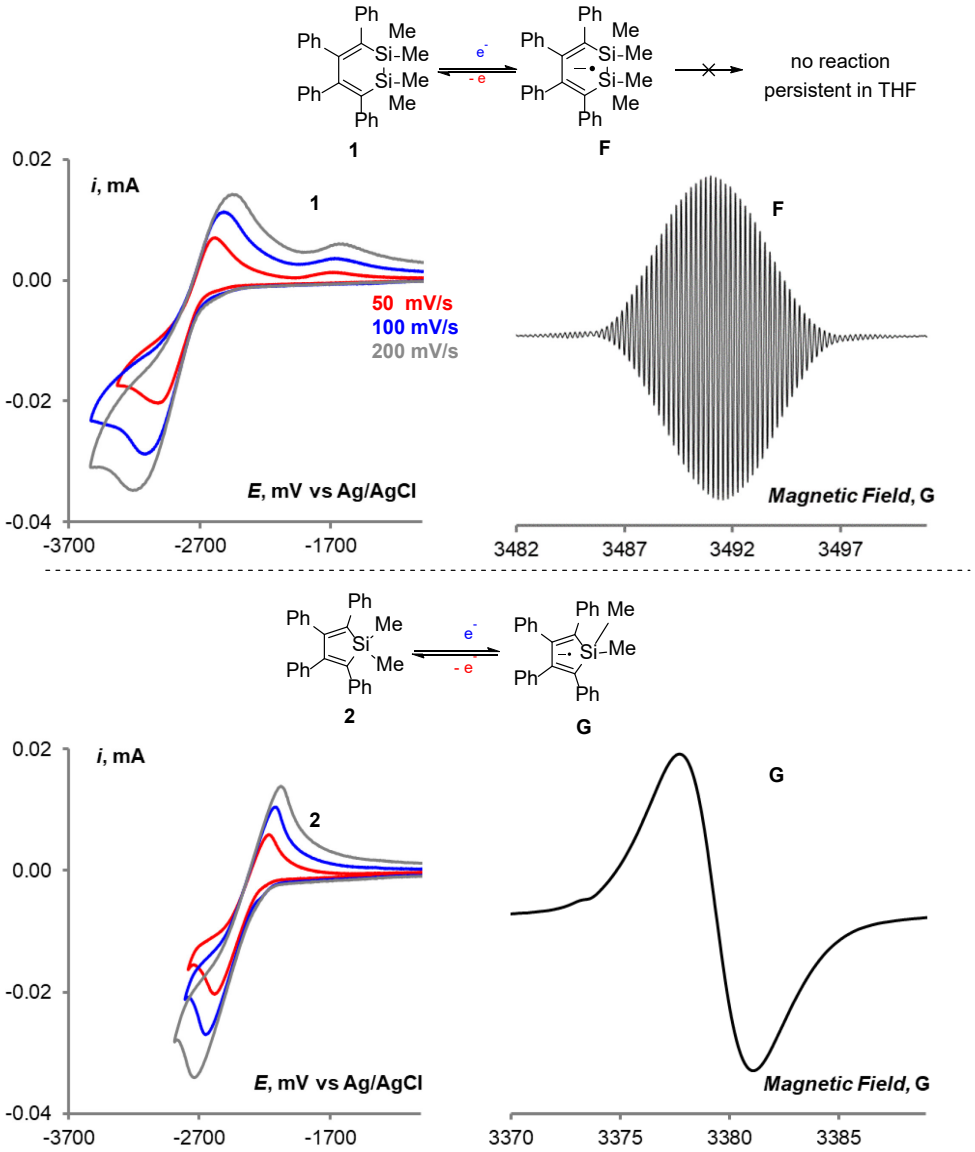

Figure 3. (Top) Reversible transformation of **1** to **F** by reduction of **1** (electrochemical or with potassium) and oxidation of **F** (electrochemical or with air, I_2, EtBr, TCNE, PCl_3) in THF. (Top left) CV curves for reduction of 5 mM of **1** at a scan rate of 50 (red), 100 (blue) and 200 (gray) mV/s . The voltammograms were recorded in 0.1 M Bu_4NBF_4/THF electrolyte (water content < 5 ppm /

* THF is a less common solvent in electroorganic practice than acetonitrile due to the high ohmic resistance of salt solutions in THF. As the result, the shape of the CV curve is greatly distorted and certain limitations and difficulties arise when performing potentiostatic electrolysis. Nevertheless, the results obtained in both media, as aprotic solvents, are very often identical but, interestingly, not in this case.

0.25 mM) on a glassy carbon disc electrode. (Top right) EPR spectra for 100 mM of **F** solution in THF/benzene 5:1 generated by reaction of **1** with 1 eq. of potassium. (Bottom) The same for **2** and **G**.

Disilacyclohexadiene radical anion is formed reversibly

The injection of a non-stoichiometric amount of electrons into solution of **1** does not initiate any self-propagating process. The persistent radical anion **F** can be obtained by reducing the corresponding reactant with alkali metals. Adding 30 mol% of potassium to a solution of **1**, is accompanied by a paramagnetic broadening of the signals in its NMR spectra. This species is persistent and can be stored in the glovebox for several weeks without changing the structure of the spectrum and its intensity. This clearly shows that a chain reaction does not occur under such conditions. Figure 3 shows the corresponding EPR spectrum of the radical anions **F** and **G**. Upon contact with air (when the vessel is opened and intensively stirred), the decay of **F** occurs within a few seconds (the intense color disappears), and NMR spectra show that it is almost completely converted back to **1**. The addition of single electron oxidizing agents such as I_2, EtBr, TCNE, PCl_3 leads to a similar result. Adding excess acid such as TsOH (a strong proton donor) is also accompanied by the preferential conversion of **F** to **1**, rather than the protonation of the radical anion as one would expect. Considering the absence of additional oxidizing agents, such as oxygen, in the TsOH solution (according to CV data), this is probably because TsOH is relatively easily reduced, thus can also act as a strong oxidizing agent for **F**.

Noteworthy is the sharp difference in the profile of the EPR spectra of **F** (g_i = 2.0035, 10 a_H = 1.29 G, 10 a_H = 0.43 G, 6 a_H = 0.2 G, a_{Si} = 11.42 G) and **G** (g_i = 1.9985, LW = 6 G). The radical anion silole **G** has the simplest form of spectrum, while the spectrum of **F** has a very rich hyperfine structure. This can be explained by the sharp difference in the structure of **1** and **2**. At first glance, both compounds have a similar butadiene backbone complemented by four aromatic substituents. However, only **2** has a relatively flat five-membered ring, whereas **1** has a strongly twisted structure of a six-membered ring, even the four butadiene carbon atoms in it are not in the same plane. Because of this, the unpaired electron in the **F** has many different intramolecular interactions. This interpretation is consistent with the results of quantum chemical simulation.

Resurrecting redox-catalytic chain with O_2: uphill electron transfer still works, but is slow.

The above data suggest that the reductive chemistry of disilacyclohexadiene is devoid of electron-catalyzed self-propagating chain reactions and transformations. However, this conclusion would be premature. In this section, we will show how, paradoxically, the catalytic cycle is promoted by the most common quenchers of radical anion chain reactions i.e., oxygen and water. It is known that oxygen is a strong electron acceptor capable of effectively removing the electron and suppress the catalytic cycle, whereas water is a proton donor which can protonate anionic intermediates. Both processes generally contribute to chain termination in radical anionic reactions.

Indeed, when a solution of $\mathbf{1}^{-\cdot}$ (**F**) in THF is opened to air with stirring, it quickly turns into solution of **1**. However, when a 3:7 $\mathbf{1}^{-\cdot}$/**1** mixture was kept under argon

atmosphere containing just 0.01% of oxygen, we observed quantitative formation of silol **2** along with dimethylsilanone oligomers in 24 hours (**Scheme *8***).

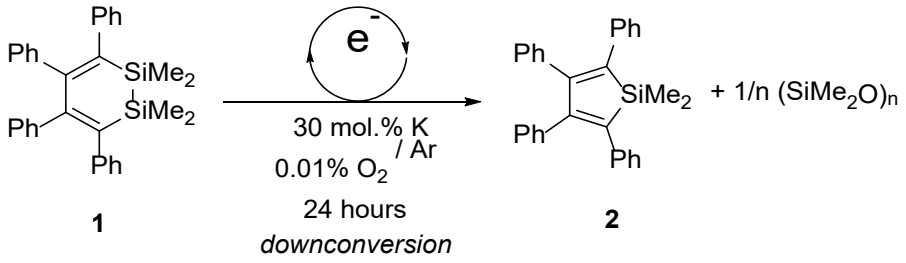

Scheme 8. Formation of **2** upon prolonged exposure of solution of **1** in the presence of a catalytic amount of electrons in an atmosphere containing low amounts of oxygen.

As we have shown earlier, there is no electron upconversion in such a cycle because the reduction potential of **1** is significantly more negative than the potential of **2**. To understand the difficulty with initiating an electron-catalyzed chain self-propagating process that would involve radical anions **F** and **G,** we can evaluate the equilibrium constant of the reaction between the neutral and one-electron reduced forms of the two compounds **1** and **2**. The 0.267 V difference in the $E^{1/2}$ reduction potentials for **1** and **2** in THF suggests that the equilibrium is strongly shifted to the left with the equilibrium constant ~ 3×10^{-5} (**Scheme *9***).

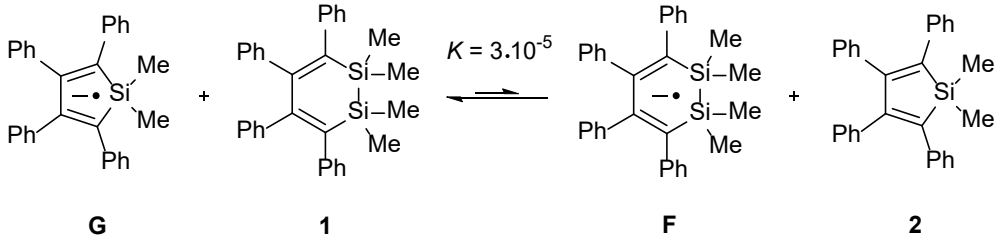

Scheme 9. Equilibrium in reversible electron transfer between **1** and **2** and their reduced forms **F** and **G**.

Thus, it would be difficult to expect the propagation of a chain reaction with these species to be efficient and the chemical reaction would still require a long time. Indeed, it takes as long as 24 hours to reach completion in this case. However, chain reaction is still possible provided that the co-product of converting **1** into **2** is quickly and irreversibly removed from the catalytic cycle. In this case, extremely thermodynamically stable siloxanes act as such stable and irreversibly formed co-product (**Scheme *8***).

Quite interesting is the difference in the behavior of the **F**/**1** system in open air vs. dry oxygen-containing argon. In open air, **1** is quantitatively reformed and no **2** is analytically detectable, while quantitative formation of **2** occurs in dry conditions. It is obvious that oxygen is a single electron oxidizing agent with respect to both **F** and **G.** An additional product in such **F**/**1** systems is superoxide $O_2^{\bullet-}$. Under aprotic conditions, $O_2^{\bullet-}$ is completely stable, and these reactions proceed reversibly (Scheme 10).

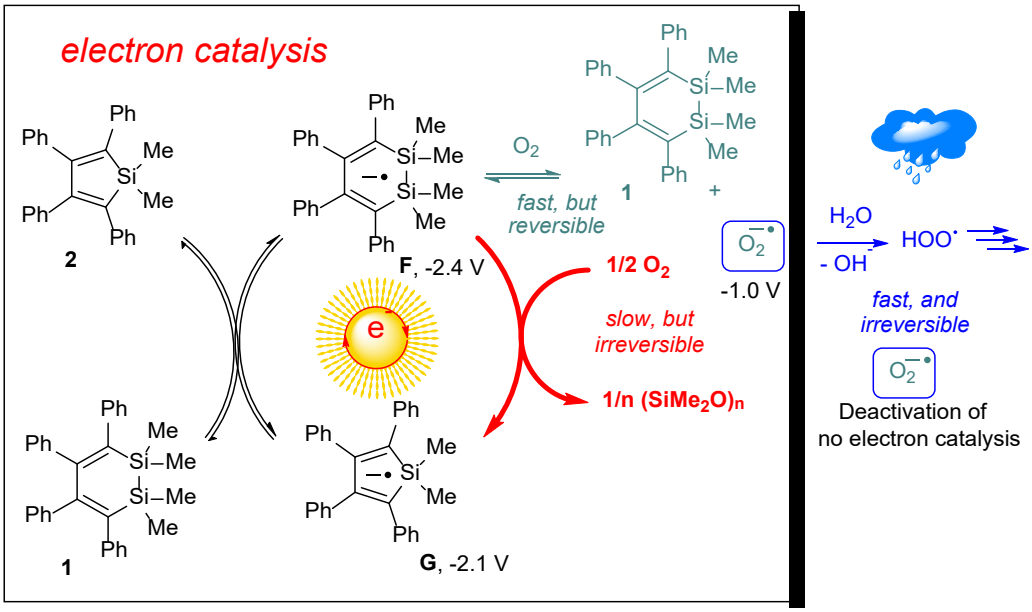

Scheme 10. The mechanism of formation of **2** during long-term (24 hours) exposure of the **F**/**1** system in the presence of 0.01% of oxygen and the absence of water, and fast (several seconds) formation of compound **1** under conditions of excess water and oxygen (with stirring in air). O_2 reduction potential from [62].

Even though the equilibrium is shifted to the right, the radical-anions **F** and **G** are formed again and again, and the electron injected into the catalytic system remains, although somewhat "cooled". At the same time, the formation of oligosiloxanes during the interaction of **F** with oxygen is a completely irreversible process which pushes the catalytic cycle to convert **1** into **2**. Thus, the electron and molecular oxygen act as unexpected allies, because they are both necessary to start and propagate the catalytic cycle. The wheel of the catalytic cycle rotates slowly but surely.

So, the presence of molecular oxygen makes it possible to "pull out" the $SiMe_2$ fragment from the six-membered ring of **1** to form a five-membered ring of **2**, due to the extreme stability of the silicon-oxygen bonds. On the other hand, a further narrowing of the ring would lead to the formation of anti-aromatic cyclobutadiene (**Scheme *11***), which is so unstable that Si-O bond formation cannot outweigh it.

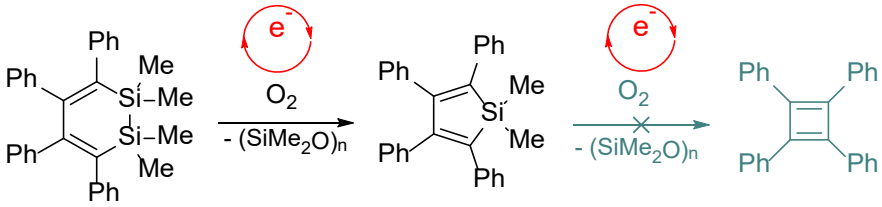

Scheme 11. Under electron catalysis conditions, O_2 can "pull out" only one $SiMe_2$ fragment from six-membered ring of **1**, but not the second. Conceptual approach to "pull" both $SiMe_2$.

The discovered process is an example of how an unfavorable (for a catalytic reaction) but reversible process can be boosted by the presence of one favorable and irreversible stage. In this scenario, even a "cold" electron can be a completely effective, albeit not fast, catalyst. Under these specific circumstances, electron down-conversion can also be compatible with a catalytic cycle.

On the other hand, when the **F**/**1** system is exposed to air (i.e., under conditions of a large excess of oxygen), the equilibrium shifts more to the right. In this case, the catalytic electron is permanently removed from the redox cycle because superoxide is extremely unstable in air which contains moisture, [63] and causes it to decompose quickly and irreversibly. Without superoxide, **1** is tolerant to air and can be stored without decomposition for years. However, **F** (its radical anionic form) is unstable under these conditions.

Resurrecting redox-catalytic chain with water: restored electron upconversion leads to faster reaction but changes the product

As seen from

Figure ***4***, a twofold molar excess of water in the solution decreases the reduction peak current of **1** approximately 5-fold, relative to the one-electron level (at a potential scan rate of 100 mV/s). A significant decrease in the current indicates that electron transfer in the presence of water initiates a *relatively fast* (< 1 s) chemical reaction which develops independently without requiring a new portion of the reducing agent. In other words, such behavior is a signature of a chain process. In contrast, the reduction peak current of **2** in the presence of water is still close to the one-electron level.

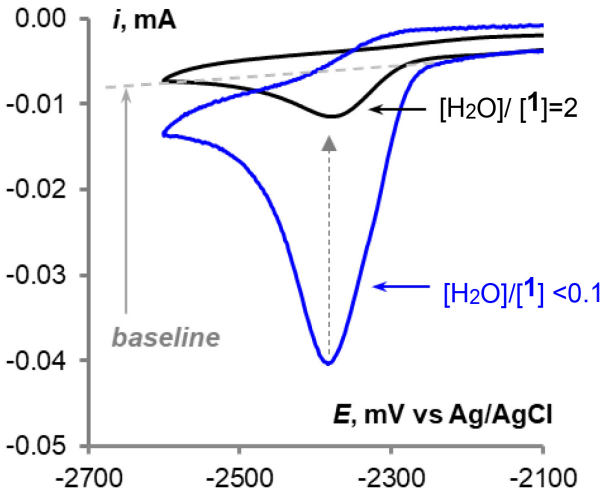

Figure 4. Effect of water on CV curves for 5 mM of **1** at a scan rate of 100 mV/s. The voltammograms were recorded in dry 0.1 M Bu_4NBF_4/MeCN electrolyte (water content < 10 ppm / 0.5 mM) and in the presence of water (200 ppm / 10 mM) on a glassy carbon disc electrode.

In this reaction, if a chain reaction is initiated by reduction of **1**, then the reduction peak current will decrease as the reduction range of **1** is repeatedly scanned. The corresponding voltametric curves obtained at 100 mV/s are shown in Figure 5. Potential scanning was performed from -2100 mV to -2600 mV and then in the reverse direction, which corresponds to 10 seconds per cycle. This scanning was repeated 10 times. For clarity, the relative values of the reduction peak currents in each subsequent scan are shown normalized to the peak current in the first scan (in solid blue, Figure 5 A). The peak current decreased approximately 4x by the second scan, and it has only 10% of the initial value in the fourth cycle. This is proportional to the decrease in the concentration of substrate **1** in the vicinity of the electrode during the chain reaction (its complete

disappearance cannot be expected due to the diffusion of the substrate from the bulk solution). For comparison, Figure *5*A also shows the oxidation peak currents versus cycle number of ferrocene (dashed line), taken as a standard of a chemically reversible process. The peak current of ferrocene does not decrease significantly with additional scans (< 3 - 4% decrease).

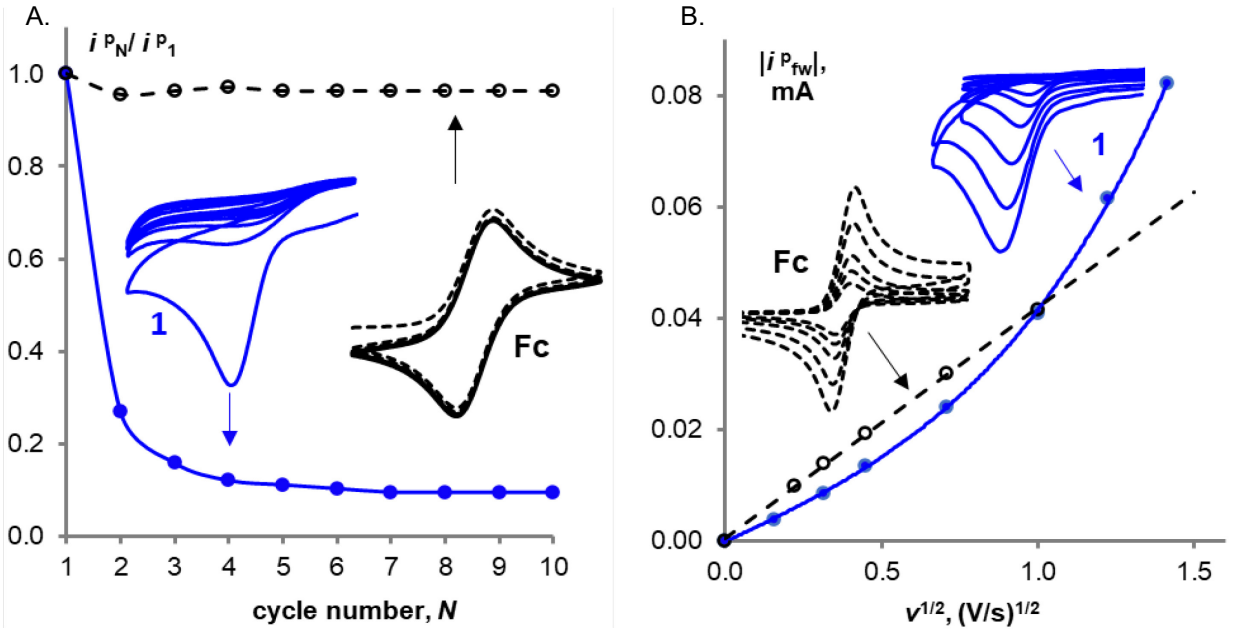

Figure 5. CV curves of reduction of 5.0 mM of **1** (the blue solid lines) and oxidation of 1.6 mM of ferrocene (the dashed lines) in 0.1 M Bu_4NBF_4/MeCN electrolyte in the presence of water (200 ppm / 10 mM) on a glassy carbon disc electrode. A. 10-fold cycling of **1** at a scan rate of 100 mV/s. The forward peak current in each cycle normalized to the current in the first scan (currents were measured from the baseline) i.e. how much the current decreases in comparison to the first scan. The current of the standard of a reversible process (ferrocene) remains almost unchanged, while for **1** the current drops significantly. B Reduction of **1** at a scan rate of 25, 100, 200, 500, 1000, 1500 and 2000 mV/s and oxidation of ferrocene at a scan rate of 50, 100, 200, 500 and 1000 mV/s. The plot of absolute values of the forward peak currents versus the square root of the potential scan rate (currents were measured from the baseline). The standard of a reversible process (ferrocene), the correlation is strictly linear, while for **1** the current increases disproportionately.

In turn, the relative decrease in the reduction peak current of **1** during an electrochemically initiated chain reaction should reduce with an increase in the potential scan rate. This is because, within a shorter time, a smaller molar amount of the substrate can react in a chain process, and thus a larger amount will participate in the stoichiometric redox reaction at the electrode. The reduction peak current of **1** versus the square root of the potential scan rate is shown in Figure 5B. For comparison, the oxidation peak current of ferrocene is also shown. For ferrocene the relationship is linear, in accordance with the Randles-Sevcik equation.[64] In the initial part of the plot the peak current of **1** is noticeably lower than that of ferrocene, despite **1** having a concentration 3 times greater. The low peak current of **1** at a low scan rate indicates that the chain reaction of **1** dominates and consumes any unreacted reactant **1** before it is able to reach the electrode. However, at a scan rate of about 1 V/s, the relative currents become equal, and at higher rates, the current of **1** becomes higher than the ferrocene current, indicating that most of reactant **1** is being reduced by the electrode instead of consumed in the chain reaction. Overall, the

non-linearity of **1** further supports that an electrochemically initiated chain reaction is occurring after the initial reduction of **1**.

To get insights into the electron-water-catalyzed version of the process, we analyzed the products of reductive electrolysis tandem gas chromatography-mass spectrometry. Electrolysis was performed at a controlled potential of reduction of **1** (-2.38 V) at a concentration of 5 mmol/L in acetonitrile with the 10 mmol/L of H_2O and the Bu_4NBF_4 supporting electrolyte on a working electrode made of a glassy carbon rod. The counter electrode and the reference electrode were separated from the catholyte by diaphragms. After passing only 0.30 F/mol of electricity, the starting compound, **1**, is not detected on the voltammetric curves and is not recorded using gas chromatography. Analysis of the resulting mixture by gas chromatography with detection of products by electron impact mass spectrometry (Supporting Information Figure S1) showed the presence of 18 peaks of oligomeric siloxanes $(SiMe_2O)_n$, which are typical products of dimethylsilanone oligomerization.[65] The peaks sequentially emerging in the mass spectra, recorded after separating the product mixture by chromatography, corresponded to particles with *n* up to 6. Peaks with higher retention times most likely corresponded to particles with higher *n* values, persistent during chromatography, but decomposing under electron impact conditions during detection. Another reaction product is tetraphenylbutene **TPB**. There were two signals, different in the retention times, but identical in mass spectra and corresponding to isomeric cis- and trans-tetraphenylbutenes in a ratio of 40:60. However, it can be concluded that isomerization occurs under the conditions of GC-MS analysis, since NMR analysis of the mixture showed quantitative conversion of **1** to **TPB** and $(SiMe_2O)_n$ (Figure S1). Other products were not observed.

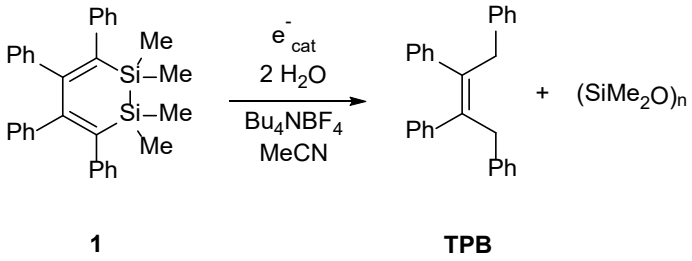

Scheme 12. Identified products of electrochemically initiated reduction of **1**.

At first glance, these products may be unexpected, since tetraphenylbutenes are formally the products of four-electron four-proton reduction of **1**. At the same time, the amount of electricity spent on their formation under electrolysis conditions is less than 10% of the “required” amount of 4 electrons per 1 product.

Similar results can be obtained in wet THF. Figure 6 shows the corresponding CV curve of reduction of **1** compared with that of separately synthesized, isolated, and characterized **TPB**. the curve of **1**, following the peak of its reduction, which is decreased relative to the one-electron level, there is a peak of reduction product in shape, potential and current identical to the **TPB** curve. After passing 0.30 F/mol of electricity through solution of **1** at its reduction potential, peak of **1** completely disappears on the CV curve and only the **TPB** peak remains. NMR and GC/MS analysis shows the presence of only **TPB** and $(SiMe_2O)_n$ in the solution (in addition to the background electrolyte).

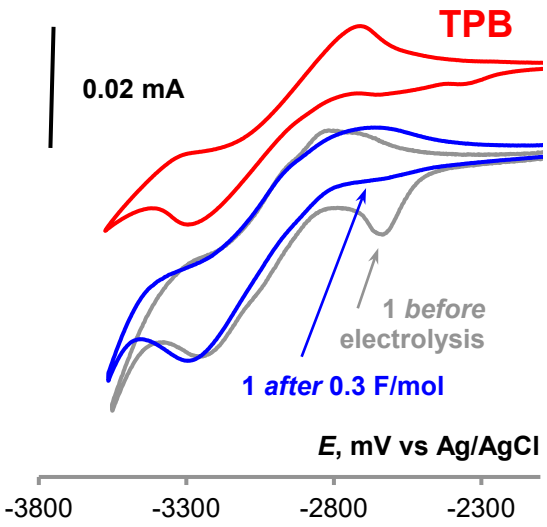

Figure 6. CV curves for 5 mM of **1** in wet 0.1 M Bu_4NBF_4/THF (water content 200 ppm / 10 mM) at a scan rate of 100 mV/s on a glassy carbon disc electrode before (gray) and after (blue) passing 0.30 F/mol of electricity at a controlled potential of reduction. For comparison, a CV curve of 5 mM **TBP** is shown (in dry 0.1 M Bu_4NBF_4/THF, water content < 5 ppm / 0.25 mM).

An experiment was also performed in which solution of **1** with 30 mol. % of potassium in the glovebox was placed in a closed vessel saturated with deuterated water vapor. The corresponding deuterated **TPB** and $(SiMe_2O)_n$ were obtained as products (**Scheme 13**). Thus, a likely participant in the cyclic process with electron upconversion provoked by water is the hydration product of **F**.

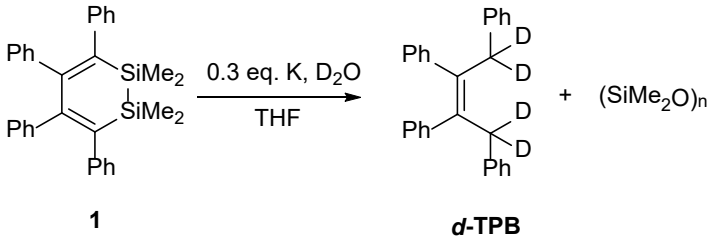

Scheme 13. Electron-catalyzed decomposition reaction of **1** under the influence of D_2O vapor.

So, water or oxygen somewhat paradoxically promotes the electron-catalyzed chain processes of decomposition of a Si-Si-containing compound. It is also interesting to note that the process is again quenched in their joint presence (Scheme 8). Undoubtedly, it would be interesting to propose a logical and substantiated mechanism for the process involving water.

It is known that the product of photolysis of **1** is the bicyclic structure **3**, which can be reversibly converted into **4** (**Scheme 14**).[66] From general considerations, it can be assumed that these compounds, as well as their radical anions, could be participants in the discovered chain process. In particular, the authors of the cited work observed **TPB** as a hydrolysis product of **4**. Since the photolysis results were obtained several decades ago, and the corresponding compounds were not fully characterized using NMR (only on ^1H nuclei), we repeated the photolysis experiment. Compounds **3** and **4** were obtained

and characterized using ^{1}H, ^{13}C and ^{29}Si NMR spectroscopy. The results indicate that in none of the experiments described above even traces of these compounds could be detected. To support this and the explanation, one can use the data of quantum chemical calculations.

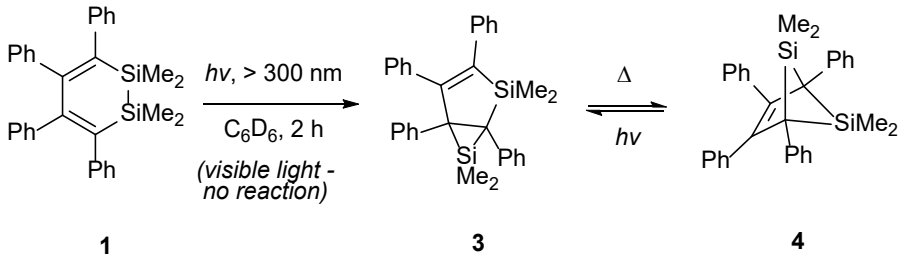

Scheme 14. Products of photochemical transformations of **1**.[66]

Computational analysis of the radical-anionic reaction

Computational analysis of the reductive pathway allowed us to draw the following conclusions about the reaction mechanism. The primary product of electron transfer to **1** is the corresponding radical anion **F**. Its reactivity determines the subsequent sequence of chemical reactions. The breaking of the weakest bond is a likely process that follows electron transfer. Such a bond in **1** is the Si-Si bond, the cleavage of which after electron transfer is typical not only in the oxidative, but also in the reductive mode.[67]

However, the Si-Si bond cleavage radical anion **F** is not predicted to be a stable intermediate (~46 kcal/mol uphill). Rearrangement to a five-membered intermediate **I** analogous to the one formed in photochemical reaction was found to be uphill by ~ 10 kcal/mol. [66] Hence, in a full agreement with the experimentally determined persistence of radical anion **F**, this species has no thermodynamically favorable escape route (Scheme 15) .

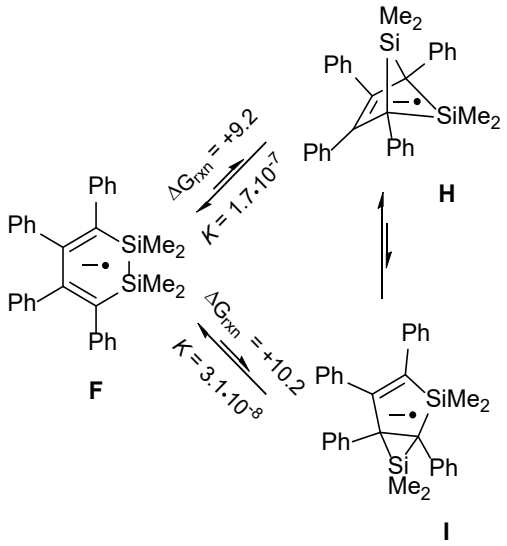

Energies in kcal/mol, PBE(D3BJ)/def2-TZVPP/Gas Phase

Scheme 15. Equilibrium between the radical anion forms of compounds **1**, **3** and **4** analogous to photochemical transformations. The transformation of the radical anion **F** into **H** and **I** is extremely thermodynamically unfavorable. The corresponding reactions are very strongly shifted towards **F**, which makes the participation of such equilibria in a fast chain process unlikely.

The situation changes, however, with the addition of water which allows a much more favorable formation of radical anion **J** which is promoted by the greater strength of Si-O bond (Scheme 16). Further reaction with water can lead to cycle opening driven by the formation of one more Si-O bond in the intermediate **L**. Presence of the extra electron weakens the alkene C=C bond in **L** and, together with the steric repulsion of the two bulky Si-group, facilitates rotation around this bond, leading to the mixture of two geometric isomers.

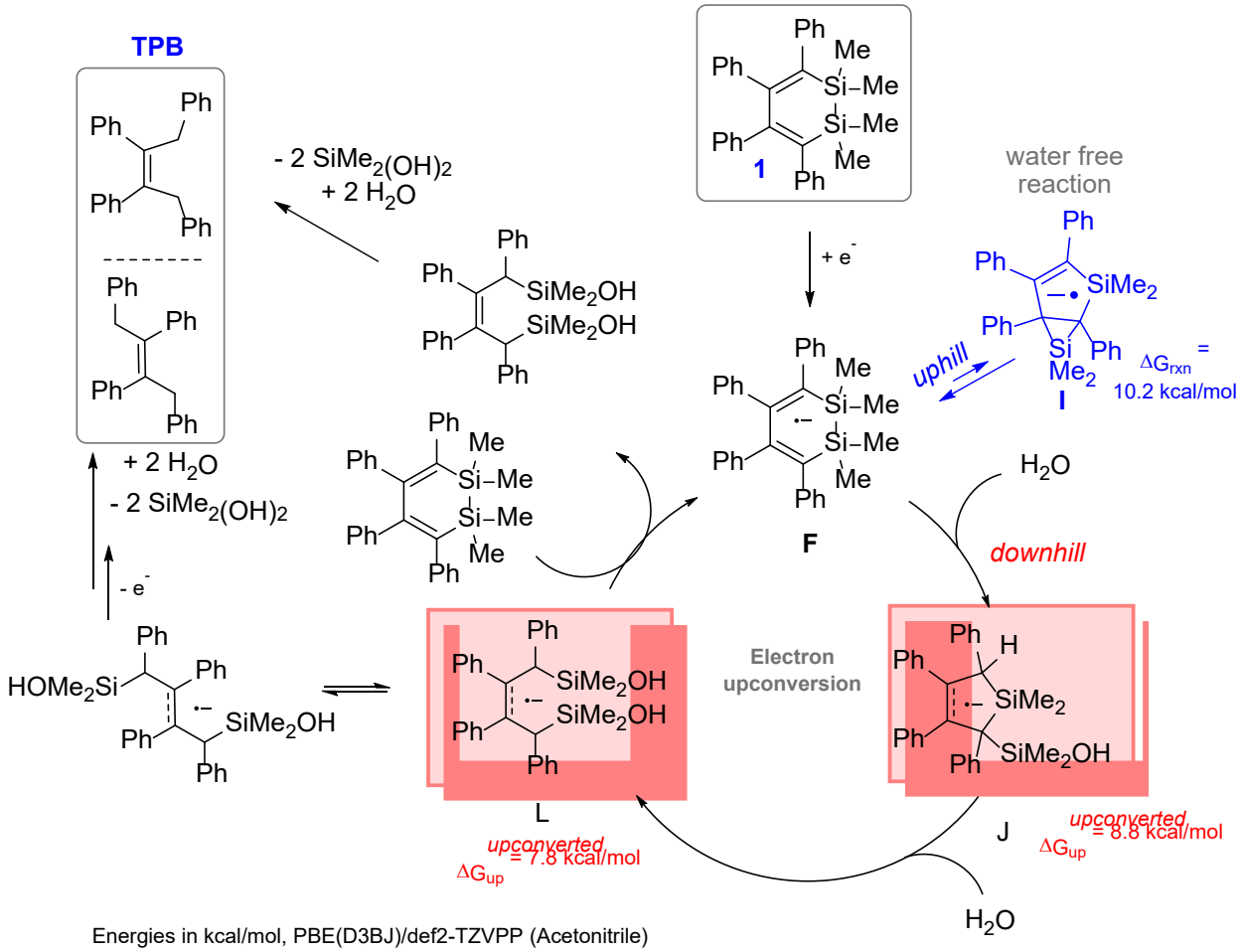

Scheme 16. Transformations of **1** in the single electron reduction regime in the presence of water.

Taking a deeper look at the mechanism of the electron-catalyzed pathway shows that reductant upconversion can occur at multiple steps throughout the reaction (Figure 7). After reduction, rearrangement of radical anion **F** results in five-membered **J**, which corresponds to an upconversion of nearly 9 kcal/mol. Next, reaction of water with **J** into **L** is favorable (ΔG = -29 kcal/mol), but **L** is even less upconverted in comparison to the starting compound **F** (ΔG_{up} = 7.8 kcal/mol). Finally, radical anionic version of the final product **TPB** from **L** is thermodynamically favorable and **TPB**$^{\bullet-}$ is also upconverted (ΔG_{up} = 9.3 kcal/mol) relative to **F** as shown in Figure 7 for the cis isomer. In the presence of water electron catalysis is unavoidable in the electron upconversion regime.

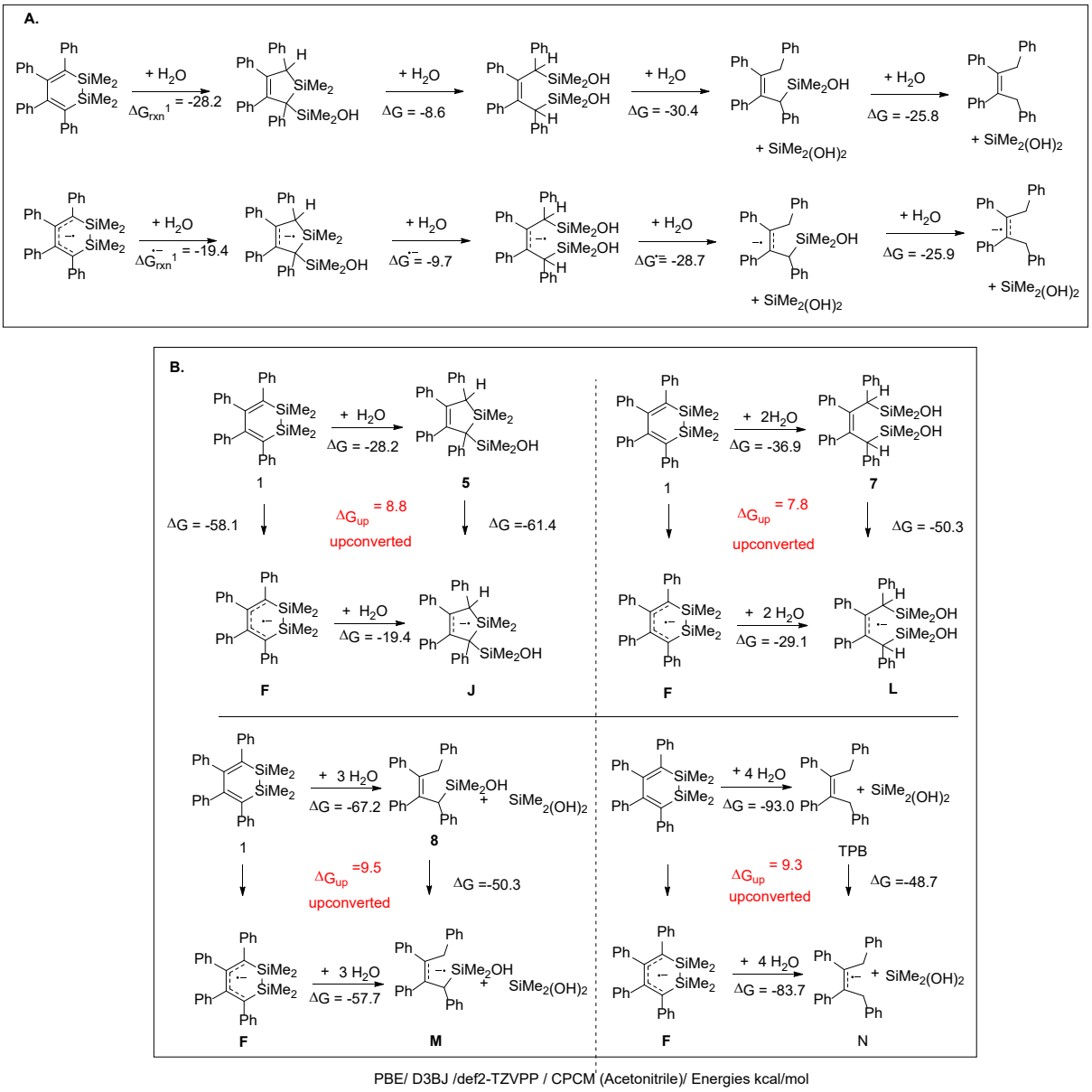

Figure 7. A. Thermodynamics of consecutive hydrolysis of neutral and radical-anionic disilacyclohexadiene **1**. B. Evaluation of reductant upconversion mediated by the single electron reduction of compound **1** in water. Each intermediate and the final product of the radical anionic pathway are upconverted relative to the starting radical-anion **F**.

An intriguing question is why the introduction of water and subsequent ability to form the Si-O bonds opens the doors for electron upconversion. One should recall that the upconversion originates from the difference in exergonicity of two reactions, i.e., the radical-anionic reaction vs. its neutral counterpart. A possible explanation is that the Si-O bond which is known to be one of the strongest chemical bonds renders the key neutral reactions (such as conversion of **1** into **5**) highly exergonic but contributes less to the respective radical anionic transformation **F→J**. A more detailed analysis of how the Si-O bond strength changes upon one-electron reduction will be the topic of our future studies.

Furthermore, computational results support that water is necessary for electron upconversion as shown by the analysis under dry conditions where molecular oxygen ($^3O_2$) can oxidize **F** to afford **2** (**Scheme 17**). First, the stubbornness of **F** to directly form **2** stems from the unfavorable thermodynamics of this process (ΔG = 32.1 kcal/mol),

supporting that oxygen is necessary for **F** to react. Although electron catalysis is present, there is no electron upconversion in the absence of water, which is expected since **G** is not a strong reductant relative to the starting material.

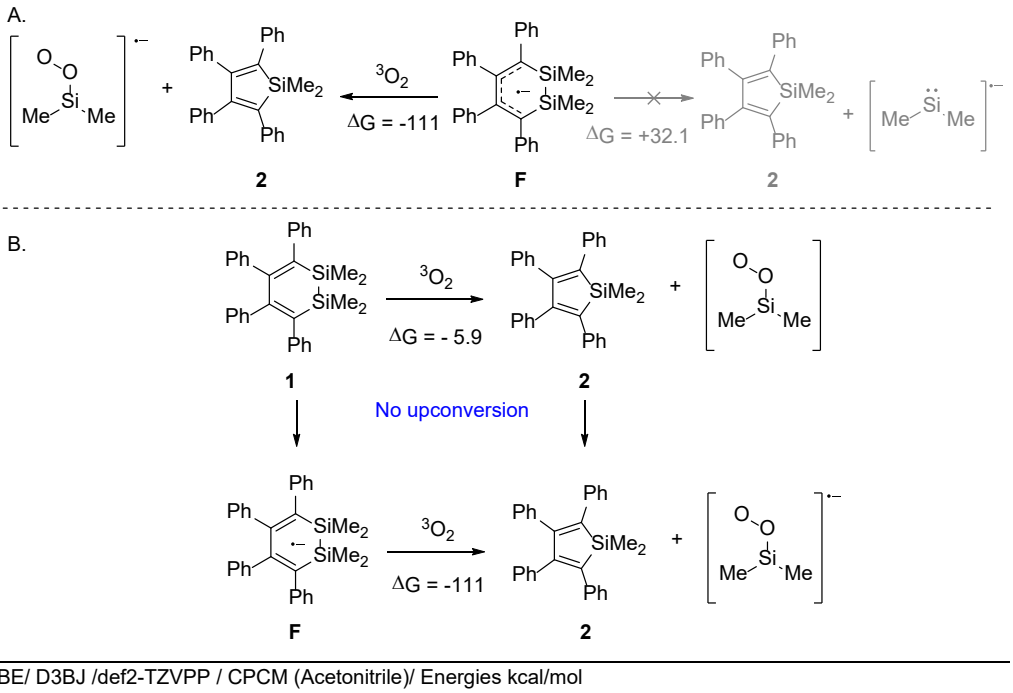

Scheme 17: A. conversion of F to 2 is more thermodynamically favorable with molecular oxygen. B. Electron upconversion is not present in the absence of water.

After upconversion was confirmed from the computed Gibbs free energies, we explored the intermediates in the pathway to determine the location of the radical anion (see details in SI Scheme S4). An alternative pathway (**Scheme 18**) can be proposed from **F** to the final product which results in the formation of intermediate **K** (ΔG_{up} = 9.5 kcal/mol) and continues on the same pathway from **K** to **M** (intermediates in Figure 7). In any case, both experimental and computational results support the involvement of water to facilitate the catalytic cycle via the upconversion. This explains the seemingly unusual formation of formal products of four-electron reduction of **1** despite the need for only catalytic amounts of electricity (0.30 F/mol).

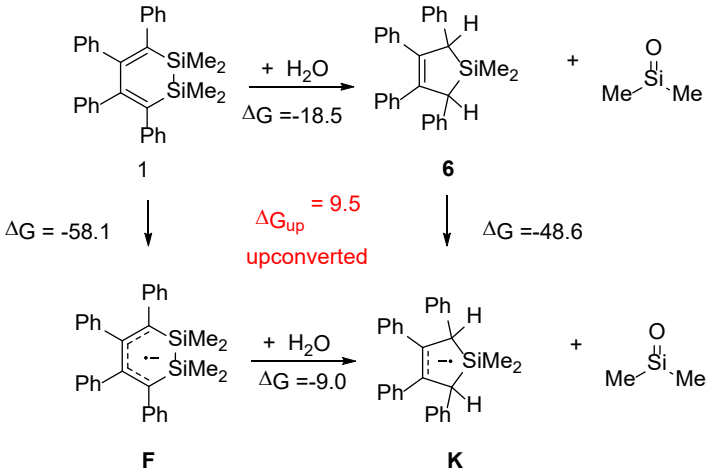

Scheme 18. Alternative pathway which forms intermediate **K** and dimethylsilanone.

4. Conclusions

The electrochemical behavior of a cyclic conjugated π-electron system containing a silicon-silicon bond shows that single electron transfer, either oxidative or reductive, breaks the Si-Si bond. However, the subsequent sequences of reactions that propagate the electron and hole catalytic cycles are fundamentally different (**Scheme 19**). In one-electron oxidation, the resulting distonic radical cation is stabilized by ring contraction leading to the formation of radical cation of silole **2.** Because it is a more powerful oxidizing agent than the radical cation of the starting diene **1**, the product radical cation oxidizes the starting compound to close a true hole-catalyzed cycle.

It is also interesting that chemical and electrochemical oxidation of the same substrate can lead to different results. In particular, catalytic cycle based on hole catalysis couldn't function in electrochemical oxidation where radical cation is quickly oxidized further. The difference between chemical (one-electron) and electrochemical (multi-electron) oxidation illustrates that multielectron pathways should be avoided in the design of true hole-catalyzed reactions. "*One hole at a time, please"* seems to be a requirement for hole catalysis.

In the case of the radical anion, the additional electron also facilitates the Si-Si bond scission but not without assistance. The initially formed radical ion is remarkably stable and persistent, so the catalytic cycle stalls. Paradoxically, the catalytic cycle can be restarted by the addition of either water or oxygen (known "antagonists" of electron catalysis). The possibility of forming strong Si-O bonds opens an alternative mechanistic path that leads to a different product, tetraphenylbutene. Because the radical anion of this product, as well as several intermediate structures, is a more powerful reductant than the radical anion of **1**, the electron-catalytic cycle is established.

Thus, both the removal and the addition of an electron to the Si-Si containing molecule initiates catalytic cycles accompanied by redox upconversion as summarized in **Scheme 19**. Hole upconversion does not require additional reagents but electron upconversion is activated only in the presence of water. The products are different and the nature of the experimentally observed path is, to a large extent, defined by the possibility of using redox upconversion. This divergent behavior suggests that redox upconversion can be used as a conceptually new tool for developing selective catalytic transformations.

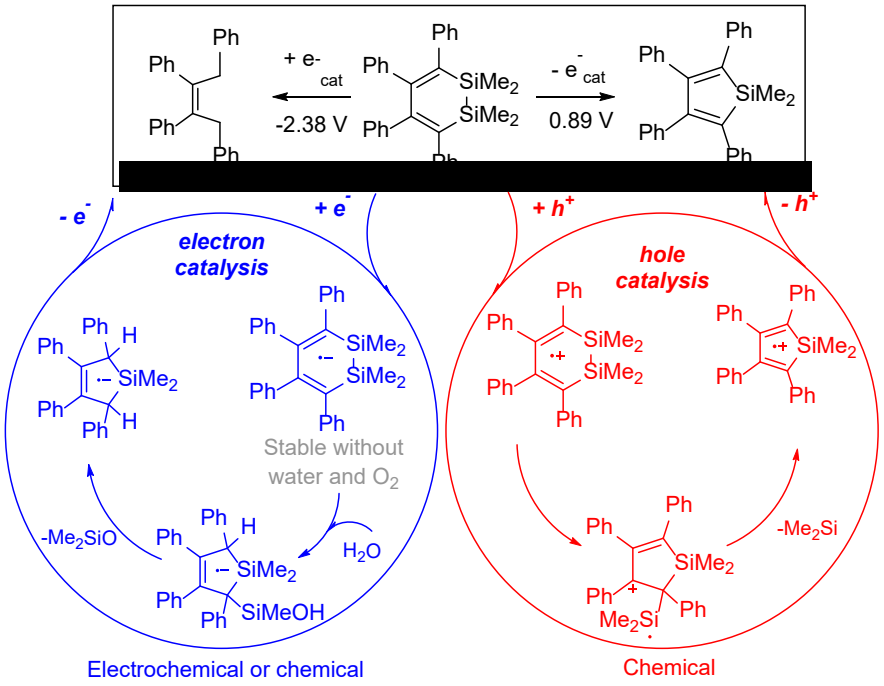

Scheme 19. Principles and differences of electron- and hole-catalyzed disilacyclohexadiene transformations.

Supporting Information

Full details of NMR and mass-spectra. Analysis of alternative mechanisms (PDF). Additional geometries and energies for all calculated structures (XYZ).The Supporting Information is available free of charge at https://pubs.acs.org/doi/10.1021/....

Acknowledgments

Experimental part of this study was supported by the Russian Science Foundation (Project No. 20-73-10234-P). The computational part of this study was sponsored by the National Science Foundation (CHE-2102579). L.K. acknowledges support by the National Science Foundation Graduate Research Fellowship under Grant No. 1449440. B.K. Chabuka acknowledges the support by the ACM SIGHPC computational and data fellowship. Crystal structure determination was performed in the Department of Structural Studies of Zelinsky Institute of Organic Chemistry, Moscow.

References

1. Möhle, S.; Zirbes, M.; Rodrigo, E.; Gieshoff, T.; Wiebe, A.; Waldvogel, S. R. Modern electrochemical aspects for the synthesis of value-added organic products. *Angew. Chem. Int. Ed.* **2018**, *57*, 6018-6041. Doi: 10.1002/anie.201712732.
2. Moeller, K. D. Using physical organic chemistry to shape the course of electrochemical reactions. *Chem. Rev.* **2018**, *118*, 4817-4833. Doi: 10.1021/acs.chemrev.7b00656.

3. Yan, M.; Kawamata, Y.; Baran, P.S. Synthetic organic electrochemical methods since 2000: on the verge of a renaissance. *Chem. Rev.* **2017**, *117*, 13230-13319. Doi: 10.1021/acs.chemrev.7b00397.
4. Yoshida, J.-i.; Kataoka, K.; Horcajada, R.; Nagaki, A. Modern strategies in electroorganic synthesis. *Chem. Rev.* **2008**, *108*, 2265-2299. Doi: 10.1021/cr0680843.
5. Zhu, C.; Ang, N.W.J.; Meyer, T.H.; Qiu, Y.; Ackermann, L. *ACS Cent. Sci.* Organic Electrochemistry: Molecular Syntheses with Potential. **2021**, *7*, 415-431. Doi: 10.1021/acscentsci.0c01532.
6. Owatari, Y.; Iseki, S.; Ogata, D.; Yuasa, J. Catalytic electron drives host–guest recognition *Chem. Sci.* **2022**, *13*, 5261-5267. Doi: 10.1039/D2SC01342H.
7. Tay, N.E.S.; Lehnherr, D.; Rovis, T. Photons or Electrons? A Critical Comparison of Electrochemistry and Photoredox Catalysis for Organic Synthesis. *Chem. Rev.* **2022**, *122*, 2487-2649. Doi: 10.1021/acs.chemrev.1c00384.
8. Luca, O. R.; Gustafson, J. L.; Maddox, S. M.; Fenwick, A. Q.; Smith, D. C. Catalysis by Electrons and Holes: Formal Potential Scales and Preparative Organic Electrochemistry. *Org. Chem. Front.* **2015**, *2*, 823-848. Doi: 10.1039/C5QO00075K.
9. Studer, A.; Curran, D.P. The electron is a catalyst. *Nature Chem.* **2014**, *6*, 765-773. Doi: 10.1038/nchem.2031.
10. Shida, N.; Imada, Y.; Nagahara, S.; Okada, Y.; Chiba, K. Interplay of arene radical cations with anions and fluorinated alcohols in hole catalysis. *Commun. Chem.* **2019**, *2*, 24. Doi: 10.1038/s42004-019-0125-4.
11. Syroeshkin, M.A.; Kuriakose, F.; Saverina, E.A.; Timofeeva, V.A.; Egorov, M.P.; Alabugin, I.V. Upconversion of reductants. *Angew. Chem. Int. Ed.* **2019**, *58*, 5532-5550 (*Angew. Chem.* **2019**, *131*, 5588-5607). Doi: 10.1002/anie.201807247.
12. Chabuka, B.K.; Alabugin, I.V. Hole Catalysis of Cycloaddition Reactions: How to Activate and Control Oxidant Upconversion in Radical-Cationic Diels–Alder Reactions. *J. Am. Chem. Soc.* **2023**, *145*, 19354-19367. Doi: 10.1021/jacs.3c06106.
13. Paulisch, T.O.; Strieth-Kalthoff, F.; Henkel, C.; Pitzer, L.; Guldi, D.M.; Glorius, F. Chain propagation determines the chemo- and regioselectivity of alkyl radical additions to C-O vs. C-C double bonds. *Chem. Sci.* **2020**, *11*, 731-736. Doi: 10.1039/C9SC04846D.
14. Elliott, Q.; Gomes, G.; Evoniuk, C. J.; Alabugin, I. V. Testing the Limits of Radical-Anionic CH-Amination: a 10-Million-Fold Decrease in Basicity Opens a New Path to Hydroxyisoindolines via a Mixed C-N/C-O-Forming Cascade. *Chem. Sci.* **2020**, *11*, 6539-6555. Doi: 10.1039/C9SC06511C.
15. Evoniuk, C. J.; Gomes, G. d. P.; Hill, S. P.; Satoshi, F.; Hanson, K.; Alabugin, I. V. Coupling N-H deprotonation, C-H activation and oxidation: metal-free C(sp3)-H aminations with unprotected anilines. *J. Am. Chem. Soc.* **2017***, 139*, 16210-16221. Doi: 10.1021/jacs.7b07519.
16. Burykina, J.V.; Shlapakov, N.S.; Gordeev, E.G.; König, B.; Ananikov, V.P. Selectivity control in thiol-yne click reactions via visible light induced associative electron upconversion. *Chem. Sci.* **2020**, *11*, 10061-10070.
17. Alvarez, E.M.; Karl, T.; Berger, F.; Torkowski, L.; Ritter, T. Late-Stage Heteroarylation of Hetero(aryl)sulfonium Salts Activated by α-Amino Alkyl Radicals. *Angew. Chem. Int. Ed.* **2021**, *60*, 13609-13613. Doi: 10.1002/anie.202103085.

18. Balycheva, V.A.; Akyeva, A.Ya.; Saverina, E.A.; Shangin, P.G.; Krylova, I.V.; Korolev, V.A.; Egorov, M.P.; Alabugin, I.V.; Syroeshkin, M.A. Electron upconversion in reactions of 1,2,4-triazoline-3,5-dione. *Russ. Chem. Bull.* **2022**, *71*, 1614-1625. Doi: 10.1007/s11172-022-3570-7.
19. Syroeshkin, M.A.; Krylov, I.B.; Hughes, A.M.; Alabugin, I.V.; Nasybullina, D.V.; Sharipov, M.Yu.; Gultyai, V.P.; Terent'ev, A.O. Electrochemical behavior of N-oxyphthalimides: Cascades initiating self-sustaining catalytic reductive N-O bond cleavage. *J. Phys. Org. Chem.* **2017**, *30*, e3744. Doi: 10.1002/poc.3744.
20. Stringle, D.L.B.; Magri, D.C.; Workentin, M.S. Efficient Homogeneous Radical-Anion Chain Reactions Initiated by Dissociative Electron Transfer to 3,3,6,6-Tetraaryl-1,2-dioxanes. *Chem. Eur. J.* **2010**, *16*, 178-188. Doi: 10.1002/chem.200902023.
21. Dell'Erba, C.; Houmam, A.; Novi, M.; Petrillo, G.; Pinson, J. Very fast, in-cage, recombination of a radical with a nucleophile. Arylazo sulfides in $S_{RN}1$ aromatic nucleophilic substitutions. *J. Org. Chem.* **1993**, *58*, 2670-2677. Doi: 10.1021/jo00062a007.
22. Mendkovich, A.S.; Ranchina, D.V.; Syroeshkin, M.A.; Demchuk, D.V.; Mikhailov, M.N.; Elinson, M.N.; Gul'tyai, V.P.; Rusakov, A.I. Mechanism of Electroreduction of the Henry Reaction Products. Electrochemically Initiated Degradation of 1-Phenyl-2-Nitroethanol. *Acta Chim. Slov.* **2014**, *61*, 246-254. http://acta-arhiv.chem-soc.si/61/61-2-246.pdf.
23. Alabugin I. V.; Zeidan, T. A. Stereoelectronic Effects and General Trends in Hyperconjugative Acceptor Ability of σ Bonds. *J. Am. Chem. Soc.* **2002**, *124*, 3175-3185. Doi: 10.1021/ja012633z.
24. Kumar, V.B.; Leitao, E.M. Properties and applications of polysilanes. *Appl. Organomet. Chem.* **2020**, *34*, e5402. Doi: 10.1002/aoc.5402.
25. Jovanovic, M.; Michl, J. Alkanes versus Oligosilanes: Conformational Effects on σ-Electron Delocalization. *J. Am. Chem. Soc.* **2022**, *144*, 463-477. Doi: 10.1021/jacs.1c10616.
26. Jovanovic, M.; Antic, D.; Rooklin, D.; Bande, A.; Michl, J. Intuitive Understanding of Delocalization in Loose and Localization in Tight Helical Conformations of an Oligosilane Chain. *Chem. Asian J.* **2017**, *12*, 1250-1263. Doi: 10.1002/asia.201700226.
27. Jovanovic, M.; Michl, J. Understanding the Effect of Conformation on Hole Delocalization in Poly(dimethylsilane). *J. Am. Chem. Soc.* **2018**, *140*, 11158-11160. Doi: 10.1021/jacs.8b05829.
28. Meenu, Km.; Bag, D.S.; Lagarkha, R.; Tomar, R.; Gupta, A.K. Functional Polysilanes and their Optical, Chiroptical and Photoluminescence Properties. *Current Organocatalysis* **2019**, *6*, 193-221. Doi: 10.2174/2213337206666190415124549.
29. Hayase, S. Polysilanes for semiconductor fabrication. *Progr. Polym. Sci.* **2003**, *28*, 359-381. Doi: 10.1016/S0079-6700(02)00034-5.
30. Su, T.A.; Li, H.; Klausen, R.S.; Kim, N.T.; Neupane, M.; Leighton, J.L.; Steigerwald, M.L.; Venkataraman, L.; Nuckolls, C. Silane and Germane Molecular Electronics. *Acc. Chem. Res.* **2017**, *50*, 1088-1095. Doi: 10.1021/acs.accounts.7b00059.

31. Nešpůrek, S.; Pospíšil, J.; Kratochvílová, I.; Sworakowski, J. Polymeric Composites Based on Polysilanes for Plastic Electronics. *Mol. Cryst. Liq. Cryst.* **2008**, *484*, 265/[631]-290/[656]. Doi: 10.1080/15421400801904682.
32. Koe, J.; Fujiki, M. *Polysilanes*. pp. 219-300, doi: 10.1016/B978-0-12-814213-4.00006-X in *Organosilicon Compounds Experiment (Physico-Chemical Studies) and Applications*, ed. by Lee, V.Ya. Academic Press, **2017**, 418 p. Doi: 10.1016/C2017-0-01409-X.
33. Kako, M.; Takada, H.; Nakadaira, Y. Electron-Transfer Reaction of 1,2-Disila-3,5-cyclohexadienes. *Tetrahedron Lett.* **1997**, *38*, 3525-3528. Doi: 10.1016/S0040-4039(97)00693-X.
34. Mochida, K.; Akazawa, M.; Fijitsuka, M.; Watanabe, A.; Ito, O. Photoinduced Electron Transfer from Tetraphenyl-Substituted 1,2-Digermacyclohexa-3,5-dienes and Related Compounds to C_{60}. *Bull. Chem. Soc. Jpn.* **1997**, *70*, 2249-2254. Doi: 10.1246/bcsj.70.2249.
35. Tang, B.Z.; Zhan, X.; Yu, G.; Lee, P.P.S.; Liu, Y.; Zhu, D. Efficient blue emission from siloles. *J. Mater. Chem.* **2001**, *11*, 2974-2978. Doi: 10.1039/B102221K.
36. Nakadaira, Y.; Sakurai, H. Synthesis and oxidation of 1,1,2,2-tetramethyl-3,4,5,6-tetraphenyl-1,2-disila-3,4-cyclohexadiene. *J. Organomet. Chem.* **1973**, *47*, 61-65. Doi: 10.1016/S0022-328X(00)92840-7.
37. CrysAlisPro. Version 1.171.41.106a. *Rigaku Oxford Diffraction*, **2021**.
38. Sheldrick, G. M. SHELXT - Integrated space-group and crystal-structure determination. *Acta Cryst.* **2015**, A71(1), 3-8. http://doi.org/10.1107/S2053273314026370
39. Sheldrick, G. M. Crystal structure refinement with SHELXL. *Acta Cryst.* **2015**, C71(1), 3-8. http://doi.org/10.1107/S2053229614024218
40. Dolomanov O.V.; Bourhis L.J.; Gildea R.J.; Howard J.A.K.; Puschmann H. OLEX2: a complete structure solution, refinement and analysis program. *J. Appl. Cryst.* **2009**, 42(2), 229-341. http://doi.org/10.1107/S0021889808042726
41. Neese, F. The ORCA program system. *WIREs Comput. Mol. Sci.* **2012**, *2*, 73-78. Doi: 10.1002/wcms.81.
42. Neese, F. Software update: The ORCA program system, version 4.0. *Wiley Interdiscip. Rev. Comput. Mol. Sci.* **2017**, *8*, 1-6.
43. Neese, F.; Wennmohs, F.; Becker, U.; Riplinger, C. The ORCA quantum chemistry program package. *J. Chem. Phys.* **2020**, *152*, 224108. DOI: 10.1063/5.0004608
44. Adamo, C.; Barone, V. Toward reliable density functional methods without adjustable parameters: The PBE0 model. *J. Chem. Phys.* **1999**, *110*, 6158-6170. Doi: 10.1063/1.478522.
45. Weigend, F.; Ahlrichs, R. Balanced basis sets of split valence, triple zeta valence and quadruple zeta valence quality for H to Rn: Design and assessment of accuracy. *Phys. Chem. Chem. Phys.* **2005**, *7*, 3297-3305. Doi: 10.1039/B508541A.
46. Grimme, S.; Antony, J.; Ehrlich, S.; Krieg, H. A consistent and accurate ab initio parametrization of density functional dispersion correction (DFT-D) for the 94 elements H-Pu. *J. Chem. Phys.* **2010**, *132*, 154104. Doi: 10.1063/1.3382344.

47. Grimme, S.; Ehrlich, S.; Goerigk, L. Effect of the damping function in dispersion corrected density functional theory. *J. Comput. Chem.* **2011**, *32*, 1456-1465. Doi: 10.1002/jcc.21759.
48. Neese, F.; Wennmohs, F.; Hansen, A.; Becker, U. Efficient, approximate and parallel Hartree-Fock and hybrid DFT calculations. A 'chain-of-spheres' algorithm for the Hartree-Fock exchange. *Chem. Phys.* **2009**, *356*, 98-109. Doi: 10.1016/j.chemphys.2008.10.036.
49. Weigend, F. Accurate Coulomb-fitting basis sets for H to Rn. *Phys. Chem. Chem. Phys.* **2006**, *8*, 1057-1065. Doi: 10.1039/B515623H.
50. Avogadro: An Open-Source Molecular Builder and Visualization Tool, version 1.2; Available online: http://avogadro.cc/ (accessed on 2 May 2021).
51. Hanwell, M.D.; Curtis, D.E.; Lonie, D.C.; Vandermeersch, T.; Zurek, E.; Hutchison, G.R. Avogadro: An advanced semantic chemical editor, visualization, and analysis platform. *J. Cheminformatics* **2012**, *4*, 17. Doi: 10.1186/1758-2946-4-17.
52. Gomes, G. d. P.; Alabugin, I. Stereoelectronic Effects: Analysis by Computational and Theoretical Methods. In *Applied Theoretical Organic Chemistry*; Tantillo, D. J., Ed.; World Scientific, **2018**, pp 451−502. Doi: 10.1142/9781786344090_0015.
53. Kako, M.; Takada, H.; Nakadaira, Y. Electron-Transfer Reaction of 1,2-Disila-3,5-cyclohexadienes. *Tetrahedron Lett.* **1997**, *38*, 3525-3528. Doi: 10.1016/S0040-4039(97)00693-X.
54. Mochida, K.; Akazawa, M.; Fijitsuka, M.; Watanabe, A.; Ito, O. Photoinduced Electron Transfer from Tetraphenyl-Substituted 1,2-Digermacyclohexa-3,5-dienes and Related Compounds to C_{60}. *Bull. Chem. Soc. Jpn.* **1997**, *70*, 2249-2254. Doi: 10.1246/bcsj.70.2249.
55. Zeitouny, J.; Jouikov, V. Reversed redox generation of silyl radicals in a four-electrode flow-through EPR spectroelectrochemical cell. *Phys. Chem. Chem. Phys.* **2009**, *11*, 7161-7170. Doi: 10.1039/B905072H.
56. Klare, H.F.T.; Albers, L.; Süsse, L.; Keess, S.; Müller, T.; Oestreich, M. Silylium Ions: From Elusive Reactive Intermediates to Potent Catalysts. *Chem. Rev.* **2021**, *121*, 10, 5889-5985. Doi: 10.1021/acs.chemrev.0c00855.
57. Lambert, J.B.; Zhao, Y.; Emblidge, R.W.; Salvador, L.A.; Liu, X.; So, J.-H.; Chelius, E.C. The β Effect of Silicon and Related Manifestations of σ Conjugation. *Acc. Chem. Res.* **1999**, *32*, 183-190. Doi: 10.1021/ar970296m.
58. Lambert, J.B.; Chelius, E.C. The β Effect of silicon in the synperiplanar geometry. *J. Am. Chem. Soc.* **1990**, *112*, 8120-8126. Doi: 10.1021/ja00178a041.
59. Alabugin, I.V.; dos Passos Gomes, G.; Abdo, M.A. Hyperconjugation. *WIREs: Comput. Mol. Sci.* **2019**, *9*, e1389. Doi: 10.1002/wcms.1389.
60. Alabugin I.V.; Manoharan, M. Effect of Double Hyperconjugation on the Apparent Donor Ability of s-Bonds: Insights From the Relative Stability of d-Substituted Cyclohexyl Cations. *J. Org. Chem.* **2004**, *69*, 9011-9024. Doi: 10.1021/jo048287w.
61. Tay, N.E.S.; Lehnherr, D.; Rovis, T. Photons or Electrons? A Critical Comparison of Electrochemistry and Photoredox Catalysis for Organic Synthesis. *Chem. Rev.* **2022**, *122*, 2487-2649. Doi: 10.1021/acs.chemrev.1c00384.

62. Li, Q. Electrochemical Reduction of Oxygen. *DPhil Thesis*, Oxford University, UK, **2014**, p. 112. https://ora.ox.ac.uk/objects/uuid:2f37a1ae-dab0-4581-a8fd-e01ce59246c4
63. The rate constant for superoxide protonation by water in acetonitrile is $1.0 \cdot 10^5$ $M^{-1}s^{-1}$: Mohammad, M.; Khan, A.Y.; Subhani, M.S.; Bibi, N.; Ahmad, S.; Saleemi, S. Kinetics and electrochemical studies on superoxide. *Res. Chem. Intermed.* **2001**, *27*, 259-267. Doi: 10.1163/156856701300356473.
64. Elgrishi, N.; Rountree, K.J.; McCarthy, B.D.; Rountree, E.S.; Eisenhart, T.T.; Dempsey, J.L. A Practical Beginner's Guide to Cyclic Voltammetry. *J. Chem. Educ.* **2018**, *95*, 2, 197-206. Doi: 10.1021/acs.jchemed.7b00361.
65. Fattakhova, D.S.; Jouikov, V.V.; Voronkov, M.G. Electrochemical oxygenation of diorganyldichlorosilanes: a novel route to generation of diorganylsilanones. *J. Organomet. Chem.* **2000**, *613*, 170-176. Doi: 10.1016/S0022-328X(00)00464-2.
66. Nakadaira, Y.; Kanouchi, S.; Sakurai, H. Photochemistry of 1,2-disila-3,5-cyclohexadienes. *J. Am. Chem. Soc.* **1974**, *96*, 5623-5624. Doi: 10.1021/ja00824a079.
67. Gilman, H.; Wu, T.C. Cleavage of the Silicon-Silicon Bond in Hexa-phenyldisilane. *J. Am. Chem. Soc.* **1951**, *73*, 4031-4033. Doi: 10.1021/ja01152a523.